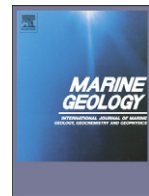




Contents lists available at ScienceDirect



Marine Geology

journal homepage: www.elsevier.com/locate/margeo

Provenance, structure, and formation of the mud wedge along inner continental shelf of the East China Sea: A synthesis of the Yangtze dispersal system

Kehui Xu ^{a,b,*}, Anchun Li ^c, J. Paul Liu ^d, John D. Milliman ^e, Zuosheng Yang ^f, Char-Shine Liu ^g, Shuh-Ji Kao ^h, Shiming Wan ^c, Fangjian Xu ⁱ

^a Department of Marine Science, Coastal Carolina University, P. O. Box 261954, Conway, SC 29528-6054, USA

^b Burroughs & Chapin Center for Marine & Wetland Studies, Coastal Carolina University, Conway, SC, USA

^c Key Laboratory of Marine Geology and Environment, Institute of Oceanology, Chinese Academy of Sciences, Qingdao, China

^d Department of Marine, Earth, and Atmospheric Sciences, North Carolina State University, Raleigh, NC, USA

^e School of Marine Science, College of William & Mary, Gloucester Point, VA, USA

^f College of Marine Geosciences, Ocean University of China, Qingdao, China

^g Institute of Oceanography, National Taiwan University, Taiwan

^h Research Center for Environmental Changes, Academia Sinica, Taiwan

ⁱ School of Geosciences, China University of Petroleum, Qingdao, China

ARTICLE INFO

Article history:

Received 13 August 2010

Received in revised form 1 June 2011

Accepted 9 June 2011

Available online xxxx

Communicated by D.J.W. Piper

Keywords:

mud wedge

sediment

sequence stratigraphy

mineralogy

East China Sea

Yangtze River

Taiwan Strait

ABSTRACT

Surficial grain-size and down-core clay mineralogical data show that sediment along the inner-most part of the continental shelf in East China Sea is mainly derived from the Yangtze River (Changjiang), spanning from the Yangtze mouth (33°N) ~1000 km southward to the southwestern corner of the Taiwan Strait (24°N). High-resolution CHIRP seismic profiles reveal an elongated mud wedge extending along the inner shelf, with a northern depocenter on the modern Yangtze delta and a southern depocenter at 27.5°N . Four distinct acoustic units are delineated within the mud wedge (from bottom up): unit I (late-Pleistocene, mainly valley fills), unit II (formed by transgressions, thin strata), unit III (11–2 kyr BP, downlapping strata) and unit IV (2–0 kyr BP, flat and opaque strata). Incised valleys, up to 15-m deep, are filled by flat-lying or inclined strata in unit I. The thin (<3 m) and acoustically transparent unit II is only seen between 30 and 26°N in water depths between 40 and 90 m. Separated by acoustically opaque strata or unconformities, units III and IV are widely distributed. During the past 11 kyr Yangtze sediment accumulation has been unsteady, showing two high and one low accumulation-rate periods. The high-accumulation period at 5–8 kyr BP may be related to maximum East Asian summer monsoon precipitation in the Yangtze basin; the other high-accumulation period, 0–2 kyr BP, probably reflects intensive human activities in the river's watershed. The low-accumulation-rate period at 2–5 kyr BP, which is seen in both northern and southern Yangtze depocenters, is probably related to low river discharge and/or intensified Taiwan Warm Current and China Coastal Current.

© 2011 Elsevier B.V. All rights reserved.

1. Introduction

Rivers provide the bulk of sediment deposited in the global oceans, approximately 15–20 billion tons/yr (Milliman and Meade, 1983; Milliman and Syvitski, 1992), but during sea-level highstands much of this sediment is sequestered in coastal and nearshore environments. More than half of global fluvial sediment is delivered by Asian rivers (Meade, 1996), such as the Ganges-Brahmaputra, Yangtze and Yellow rivers. Historically the Yangtze and Yellow rivers have transferred ~480 and ~1000 million tons/yr (Mt/yr) to the East China Sea (ECS), Bohai

Sea, and Yellow Sea (Fig. 1), representing ~10% of global sediment discharge.

The fate of this bulk sediment from the Yangtze and Yellow rivers is largely controlled by counter-clockwise circulation in the ECS and Yellow Sea (Fig. 1). The dominating current is Kuroshio Warm Current, which flows along the eastern edge of the ECS and pushes the Yellow Sea Warm Current northward along western Korea (Fig. 1). Completing this circulation, the China Coastal Current flows southward along the western side and brings colder water into the southwestern ECS.

Debouching onto a wide (>600 km) epicontinental shelf, the Yangtze and Yellow rivers have formed three distinct mud deposits in the ECS: a mud wedge along the entire inner shelf, a mud patch southwest of the Cheju Island, and a deeper (>1000 m water depth) deposit in the Okinawa Trough (Fig. 2). While most of the ECS floor is covered by sand, the inner shelf (landward of ~80-m isobath) is

* Corresponding author at: Department of Marine Science, Coastal Carolina University, P. O. Box 261954, Conway, SC 29528-6054, USA. Tel.: +1 843 349 6494; fax: +1 843 349 4042.

E-mail address: kxu@coastal.edu (K. Xu).

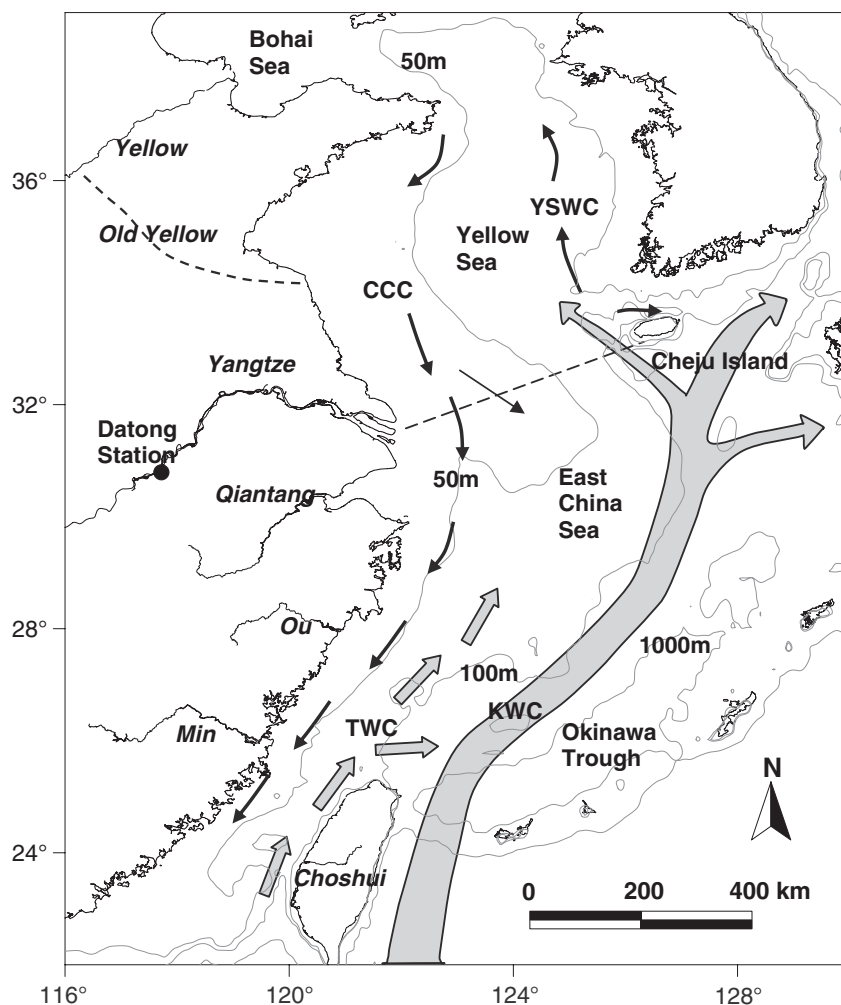


Fig. 1. Bathymetry and major currents in the East China Sea and Yellow Sea. KWC, Kuroshio Warm Current; TWC, Taiwan Warm Current; CCC, China Coastal Current; and YSWC, Yellow Sea Warm Current. Dashed straight line from Yangtze mouth to Cheju Island is the dividing line between the East China Sea and Yellow Sea. The old Yellow River entered the Yellow Sea from 1128 to 1855 AD (dashed course).

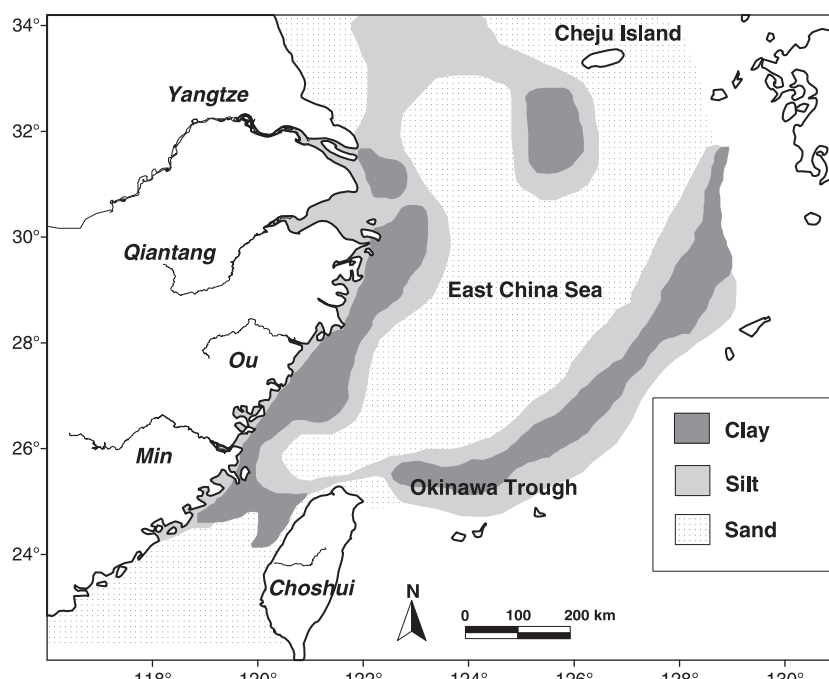


Fig. 2. Surficial sediment types in the East China Sea. There are three major mud deposits: inner shelf, southwest of Cheju Island, and deeper Okinawa Trough. Middle and outer shelf surficial sediments are primarily relict sands.

mostly covered with mud (Fig. 2). This inner-shelf mud wedge is perhaps the most extensive deposit in southeastern Asia, extending 1000 km from the Yangtze mouth southward into the Taiwan Strait (Fig. 2).

A large number of geological and geophysical studies have been made in the ECS to document the fate of the Yangtze-derived sediment, in particular near the Yangtze mouth (Milliman et al., 1985; Chen and Stanley, 1993; Hu et al., 1998; Chen et al., 2000; Hori et al., 2001a, 2002; Chen et al., 2003; Lin et al., 2005; Yi et al., 2006; Li et al., 2009; Liu et al., 2010b; Wang et al., 2010b) and in the middle shelf (Liu et al., 2000; Berne et al., 2002; Liu et al., 2007b). During the past five years there has been increasing interest on the inner shelf. The elongated inner-shelf mud wedge was first documented by Liu et al. (2006) based on high-resolution CHIRP seismic profiles. Using eight across-shore seismic profiles, Liu et al. (2007a) subsequently reported northern (on the modern Yangtze delta) and southern (at ~27.5°N) depocenters of the mud wedge, discussed the development history of Yangtze deposit, and proposed the preliminary sediment budget. Xu (2006) and Xu et al. (2009a) have shown that fine-grained surficial sediment in the western Taiwan Strait tends to be derived from the Yangtze River, whereas silt and sand along the eastern Taiwan Strait come from Taiwan. In addition, Liu et al. (2008a) have shown the presence of a northward prograding sand–silt-dominated subaqueous delta extending from the Choshui River (western Taiwan) into the northern Taiwan Strait. Using sediment and morphological data, Liao et al. (2008) reported that sandy bodies in the eastern Taiwan Strait can be divided into sand ridge, shoal and sheet provinces, but short-term changes in seafloor character can occur in response to typhoon-generated floods from Taiwanese rivers (Milliman et al., 2007).

Despite these studies, our knowledge of this inner-shelf sediment dispersal system in the ECS has been limited, especially along the middle and southern part of the mud wedge (south of 31°N). 1) Due to relatively-short penetration depths (normally <5 m) of typical piston and gravity cores, many past coring sites were selected at the near-pinch-out parts of the mud wedge in order to reach as deeply as possible into its basal strata (e.g., Xiao et al., 2004, 2005). Such coring unfortunately was not long enough to penetrate the >40-m-thick depocenters in the mud wedge. 2) With limited radiocarbon dates, the developmental history of southern depocenter of mud wedge also has been poorly understood. 3) Most previous studies were based on two-dimensional cross-shore CHIRP seismic profiles, but three-dimensional analysis (e.g., fence diagrams) of cross- and along-shore seismic profiles was needed to investigate this complex dispersal system. 4) The southern boundary of the inner-shelf mud wedge was defined on the basis of a single profile (Liu et al., 2007a), the actual and the south extent remaining unclear. 5) Sand and clay mineralogies allowed Xu et al. (2009a) to differentiate Yangtze-derived clay from Taiwan-derived silt/sand in surficial sediment, but no down-core mineralogical data have been reported. You et al. (1993) published some clay mineralogical data derived from several gravity cores collected along the western Taiwan Strait, but they did not compare them with clay data from nearby rivers (e.g., Min or Choshui rivers). Delineating the southern boundary of inner-shelf mud wedge is critical since it allows one to estimate both the Yangtze and Taiwan sediment budgets.

Based on CHIRP seismic data collected by J.P. Liu et al. in 2003 and 2004, a 60.2 m borehole EC2005 was collected in 2005 by Shanghai Marine Petroleum Bureau at the southern depocenter of inner-shelf mud wedge in a water depth of 36 m (Fig. 3). A total of 16 new AMS radiocarbon dates derived from this core were reported by Xu et al. (2009b). In addition, two other giant piston cores, MD06-3039 and MD06-3040, 19.2 and 8.1 m long, respectively, were recovered at the same location by Laj et al. (2006) in 2006 (Fig. 3); 9 radiocarbon dates from these two cores were then reported by Zheng et al. (2010). Liu et al. (2010a) recently reported 17 new radiocarbon dates from a 35.6-m-long borehole core ECS-0702 collected at 22-m water depth in the southeastern Yangtze subaqueous delta. Wang et al. (2010a) also

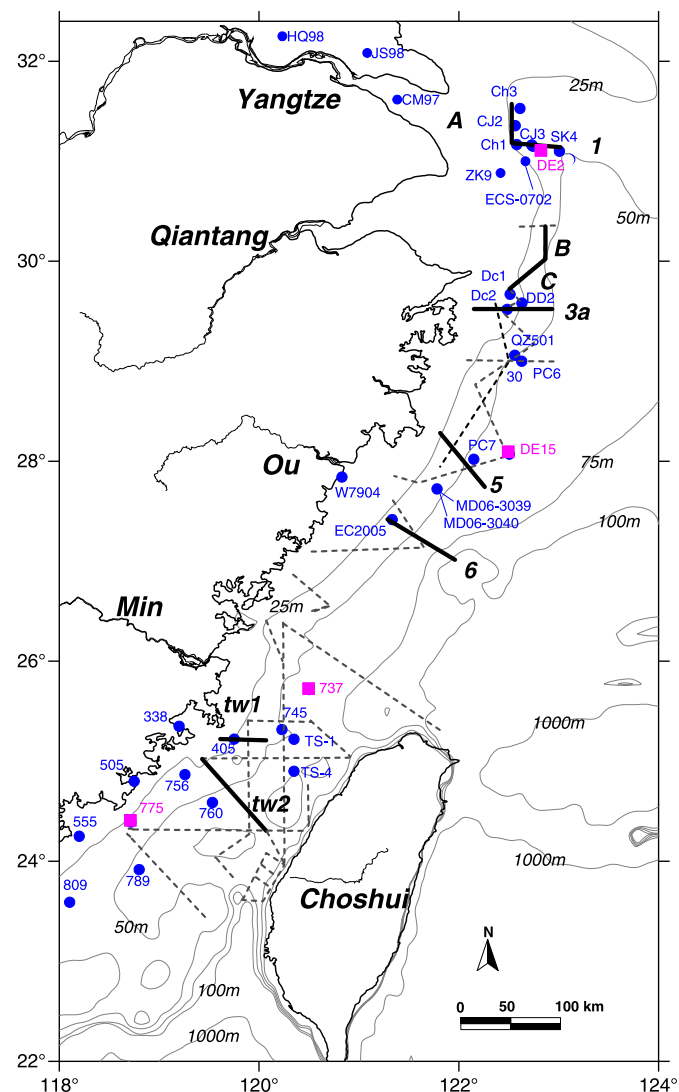


Fig. 3. Spatial distribution of ~3000 km of CHIRP seismic profiles collected in 2003–2006, as well as gravity and box cores in the East China Sea. Core DE2, DE15, 737 and 775 (purple squares) are used for clay mineralogical analyses. Bold profiles are shown in Figs. 8–11. (For interpretation of the references to color in this figure legend, the reader is referred to the web version of this article.)

documented 12 radiocarbon dates from a 55-m-long core ZK9 in the Yangtze subaqueous delta at a water depth of 12.5 m. These new radiocarbon dates, together with other published dates compiled from many papers (Table 1), represent a total of 130 radiocarbon dates from the entire inner shelf used in this study (Fig. 3).

In this paper we focus on provenance and stratigraphy. The provenance part is based on mineralogical and grain-size analyses. A total of 19 new and 14 published (You et al., 1993) down-core mineralogical data were used to identify sediment source. In addition, a total of 59 river and marine samples were collected from Min and Ou rivers (mainland China), Taiwan Island, and Taiwan Strait (Fig. 4). New grain size data derived from these 59 samples were used to examine the mixing of muddy Yangtze and sandy Taiwanese sediment. The stratigraphy part of the paper is based on the lithology of cores, 35 shore-normal and shore-parallel seismic profiles, combined with 130 published radiocarbon dates.

The objectives of this study are: 1) to identify the dominant provenance of the inner-shelf mud wedge in the ECS and to delineate the southern boundary of inner-shelf Yangtze mud wedge and the northern boundary of Taiwan-derived sediments; 2) to examine the

Table 1

Selected radiocarbon dates from cores along in the inner shelf of East China Sea.

Core (from north to south)	Lat. (°)	Lon. (°)	Elevation of core top (m)*	Core depth (m)	Elevation of carbon sample (m)*	Dating materials	14C age (yr)		Calibrated age (yr BP)			Source			
							14C age (yr)	±1σ	Cal. BP	Lower range	Upper range				
CM97	31.62	121.38	2.48	9.31	-6.83	M.S.	1840	50	1383	1312	1435	Hori et al. (2002)			
				20.48	-18.00	M.S.	1510	50	1062	993	1127				
				20.53	-18.05	M.S.	1850	50	1393	1328	1450				
				20.73	-18.25	M.S.	1690	50	1246	1197	1292				
				22.65	-20.17	M.S.	4050	50	4077	3985	4145				
				23.92	-21.44	M.S.	4580	50	4795	4763	4851				
				24.63	-22.15	M.S.	5150	50	5514	5468	5569				
				25.43	-22.95	M.S.	6010	50	6424	6358	6486				
				27.34	-24.86	M.S.	7040	50	7526	7478	7570				
				28.99	-26.51	M.S.	8400	50	9005	8944	9082				
				40.20	-37.72	M.S.	9740	50	10,594	10,538	10,642				
				61.06	-58.58	M.S.	10,820	50	12,288	12,179	12,377				
JS98	32.08	121.08	4.20	9.70	-5.50	M.S.	1640	40	1204	1166	1254	Hori et al. (2002)			
				17.50	-13.30	M.S.	3200	40	3007	2934	3071				
				19.87	-15.67	M.S.	2860	40	2627	2571	2706				
				21.69	-17.49	M.S.	2890	40	2672	2643	2731				
				25.30	-21.10	M.S.	4750	30	4989	4920	5043				
				27.45	-23.25	M.S.	6640	40	7178	7141	7233				
				27.64	-23.44	M.S.	6640	60	7171	7107	7249				
				28.57	-24.37	M.S.	6070	80	6496	6402	6592				
				29.40	-25.20	M.S.	6050	60	6472	6395	6545				
				33.36	-29.16	M.S.	7410	70	7871	7801	7944				
				34.60	-30.40	M.S.	7220	60	7686	7615	7746				
				35.30	-31.10	M.S.	7500	60	7961	7897	8025				
				36.40	-32.20	M.S.	8660	120	9309	9187	9461				
				44.55	-40.35	M.S.	9510	90	10,365	10,262	10,466				
				45.46	-41.26	M.S.	9780	80	10,661	10,539	10,752				
				52.55	-48.35	M.S.	11,900	80	13,350	13,273	13,423				
HQ98	32.25	120.23	5.91	0.70	5.21	Snail Shell	180	50	520	470	570	Hori et al. (2002)			
				4.70	1.21	M.S.	4120	50	4180	4088	4250				
				5.50	0.41	M.S.	5230	30	5594	5567	5625				
				6.15	-0.24	M.S.	5580	60	5976	5895	6047				
				13.30	-7.39	M.S.	4310	50	4439	4377	4512				
				23.20	-17.29	M.S.	5310	60	5674	5594	5726				
				28.60	-22.69	M.S.	6830	70	7349	7286	7414				
				30.12	-24.21	M.S.	8130	70	8614	8507	8717				
				42.75	-36.84	M.S.	9080	120	9823	9623	10,004				
				48.32	-42.41	M.S.	10,250	80	11,245	11,159	11,317				
				52.65	-46.74	Plant	10,450	70	11,552	11,367	11,702				
				53.80	-47.89	Plant	10,550	90	11,758	11,612	11,964				
ZK9	30.88	122.42	-12.50	6.62	-19.12	Shell	1504	33	1054	998	1105	Wang et al. (2010a)			
				14.57	-27.07	Shell	5086	27	5452	5407	5524				
				14.85	-27.35	Shell	8005	36	8461	8411	8505				
				15.12	-27.62	Shell	8119	38	8585	8526	8635				
				28.5	-41.00	Wood	8191	48	8694	8591	8764				
				31.13	-43.63	Plant	9171	43	9981	9900	10,083				
				36.7	-49.20	Plant	9441	37	10,285	10,224	10,334				
				42	-54.50	Plant	11,335	56	12,797	12,700	12,881				
ECS-0702	31.00	122.67	-22.00	0.74	-22.74	G.	500	40	122	55	149	Liu et al. (2010a)			
				1.75	-23.75	G.	610	40	256	225	302				
				3.87	-25.87	M.S.	790	40	432	397	483				
				7.89	-29.89	M.S.	880	40	499	470	525				
				9.03	-31.03	G.	1000	40	584	546	621				
				10.24	-32.24	M.S.	1620	40	1186	1143	1241				
				11.07	-33.07	G.	1810	40	1349	1299	1385				
				12.34	-34.34	G.	2480	40	2139	2058	2206				
				13.82	-35.82	G.	2640	40	2326	2280	2380				
				16.12	-38.12	M.S.	6110	40	6539	6483	6600				
				18.99	-40.99	M.S.	6630	40	7167	7129	7231				
				24.65	-46.65	M.S.	8350	40	8937	8878	9000				
				31.96	-53.96	Plant	10,370	50	11,381	11,242	11,414				
				31.17	122.58	-24.00	36.20	-60.20	Mud	10,700	125	12,062	11,857	12,343	Qin et al. (1987)
				31.53	122.61	-31.00	31.30	-62.30	Mud	10,475	300	11,687	11,202	12,106	
				31.36	122.57	-36.00	30.70	-66.70	Mud	15,460	420	18,219	17,811	18,684	
				31.10	123.01	-50.00	0.38	-50.38	Molluscs	1230	40	771	714	821	
Dc1	29.67	122.51	-28.00	19.00	-47.00	Mud	11,510	570	12,932	12,322	13,679	Qin et al. (1987)			
				29.52	122.48	-28.00	31.40	-59.40	Mud	11,520	690	12,936	12,051	13,797	
				29.58	122.63	-43.50	0.49	-43.99	B.S.	640	40	288	244	333	
							1.09	-44.59	forams	1420	30	964	921	996	
							2.03	-45.53	forams	1980	25	1538	1501	1581	
							2.31	-45.81	forams	6100	55	6528	6460	6603	
DD2	29.67	122.51	-28.00	2.55	-46.05	forams	6020	60	6437	6359	6511	Xiao et al. (2004)			

Table 1 (continued)

Core (from north to south)	Lat. (°)	Lon. (°)	Elevation of core top (m)*	Core depth (m)	Elevation of carbon sample (m)*	Dating materials	14C age (yr)		Calibrated age (yr BP)			Source
							14C age (yr)	± 1σ	Cal. BP	Lower range	Upper range	
PC6	29.00	122.63	−56.70	0.75	−57.45	forams	1830	25	1364	1325	1397	Xiao et al. (2005)
				1.79	−58.49	forams	4860	35	5169	5114	5258	
				2.79	−59.49	forams	6550	35	7070	7019	7134	
				3.49	−60.19	forams	6960	35	7463	7423	7493	
30	28.98	122.54	−54.00	2.20	−56.20	forams	3410	40	7611	7572	7646	Liu et al. (2007a)
				1.70	−65.70	Mud	6600	300	7075	6779	7407	Yu and Li (1992)
PC7	28.02	122.15	−64.00	5.50	−69.50	Mud	7700	300	8179	7844	8473	
				4.29	−60.99	forams	7140	40	3287	3238	3341	
				5.50	−69.50	forams	3410	40	1800	1760	1849	
				4.01	−40.01	forams	1740	25	4370	4298	4423	Xu et al. (2009b)
EC2005	27.42	121.33	−36.00	5.57	−41.57	forams	1900	40	1290	1263	1313	
				6.69	−42.69	forams	2200	25	1445	1394	1500	
				8.97	−44.97	forams	4260	40	1785	1760	1849	
				12.33	−48.33	forams	4870	45	5176	5114	5272	
				17.85	−53.85	forams	5250	40	5612	5572	5647	
				23.33	−59.33	forams	5500	45	5883	5828	5945	
				25.01	−61.01	forams	5610	35	6001	5932	6054	
				28.04	−64.04	forams	6750	40	7281	7233	7326	
				30.21	−66.21	forams	6980	30	7479	7436	7507	
				31.41	−67.41	forams	9980	40	10,966	10,894	11,093	
				33.09	−69.09	forams	10,700	90	12,075	11,918	12,270	
				36.77	−72.77	forams	10,800	40	12,252	12,180	12,343	
MD06 – 3039	27.72	121.78	−46.00	41.02	−77.02	peat	11,200	210	12,695	12,526	12,956	
				50.85	−86.85	forams	13,000	85	14,818	14,605	15,082	
				55.73	−91.73	forams	13,750	65	16,469	16,272	16,732	
				1.40	−47.40	B.S.	627	221	278	77	433	Zheng et al. (2010)
				2.10	−48.10	B.S.	1217	22	752	716	783	
				2.82	−48.82	B.S.	1741	21	1290	1265	1311	
				4.75	−50.75	B.S.	3396	22	3277	3240	3319	
				6.63	−52.63	B.S.	3917	25	3896	3850	3940	
				11.51	−57.51	B.S.	4992	34	5351	5294	5396	Zheng et al. (2010)
				13.63	−59.63	B.S.	5788	41	6216	6178	6261	
MD06 – 3040	27.72	121.78	−46.00	16.11	−62.11	B.S.	7205	36	7666	7616	7704	
				19.12	−65.12	B.S.	9479	33	10,325	10,259	10,376	
				27.84	120.83	−2.00	19.60	−21.60	10,598	9894	11,207	Ye et al. (1981)
				25.72	120.50	−62.00	5.95	−67.95	11,099	10,731	11,325	Lan et al. (1993)
W7904 737 745	25.32	120.23	−48.00	2.70	−50.70		7800	149	8260	8102	8409	
				4.60	−52.60		9173	174	9934	9709	10,169	
				760	24.59	119.53	−56.00	0.90	12,572	14,714	14,842	
				2.70	−58.70		12,572	347	14,238	14,714	14,842	
789	23.92	118.80	−54.00	0.90	−54.90		14,497	349	17,235	16,852	17,605	
				2.15	−56.15		14,588	224	17,298	16,999	17,546	
				1.00	−43.00		3349	130	3194	3031	3359	
				2.50	−44.50		13,927	219	16,540	16,205	16,925	
775	24.39	118.72	−40.00	4.00	−46.00		27,746	559	31,711	31,140	32,170	
				0.80	−40.80		25,046	514	29,462	28,980	30,175	
				2.40	−42.40		37,058	943	41,530	40,838	42,374	
				2.70	−47.70		11,247	331	12,703	12,360	13,125	
756	24.87	119.26	−45.00	5.50	−50.50		17,498	577	20,391	19,804	21,096	
				1.20	−26.20		8513	277	9112	8770	9456	
				2.10	−27.10		11,174	288	12,630	12,344	12,989	
				2.00	−4.00		2884	201	2623	2349	2839	
405	25.22	119.75	−25.00	2.20	−4.20		3168	166	2986	2773	3171	
				0.90	−2.90		4426	210	4585	4294	4846	
				1.60	−3.60		5461	192	5844	5615	6041	
				5.00	−65.00		5500	300	5884	5574	6220	Chien and Leu (1984)
TS1 TS4	24.90	120.35	−68.00	5.00	−73.00		5500	300	5884	5574	6220	

Locations of cores are in Fig. 3.

All radiocarbon ages were calibrated using CALIB6.0.1, which is available at <http://intcal.qub.ac.uk/calib/>.

The calibration date set was Marine 04, which includes a constant average global reservoir age of 400 yr.

Lon. = longitude, Lat. = latitude, M.S. = Molluscan Shell, G. = Gastropod, B.S. = Bivalve Shells.

BP = Before Present, where present is 1950 A.D.

Dating materials for Ye et al. (1981), Lan et al. (1993), and Chien and Leu (1984) were not reported in the references.

* Indicates the elevation above modern sea level, and negative values indicate below sea level.

complex structure and formation of the stratigraphic record using three-dimensional seismic fence diagrams; 3) to study the variation of sediment accumulation in the northern and southern depocenters of this mud wedge, with a focus on high and low accumulation rates as well as truncations; and 4) to investigate the formation of the system tracts under the control of sea level and paleo-environment since Last Glacial Maximum.

Many past studies were regionally focused on the Yangtze Delta, inner ECS shelf or the Taiwan Strait. By synthesizing seismic, granulometric, lithological, mineralogical and radionuclide data, this study strives to provide a comprehensive synthesis of the entire Yangtze dispersal system (from 33 to 23°N) that will be of interest of international scientists studying large and small-mountainous rivers dispersal systems around the world.

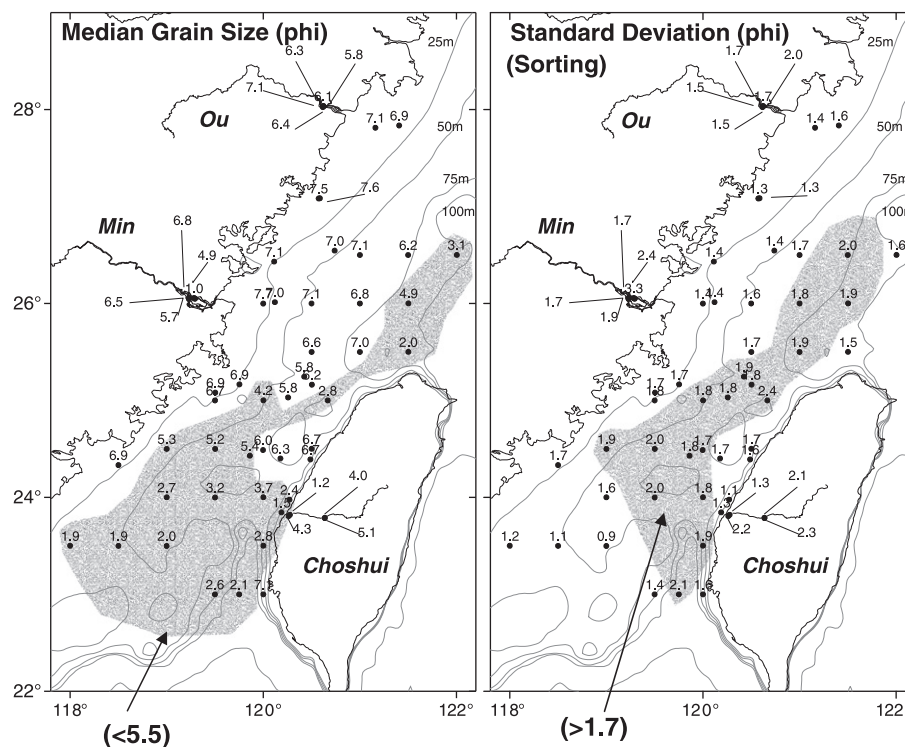


Fig. 4. Median grain size and standard deviation (in phi) of sediment from the Min, Ou and Choshui rivers as well as surficial sediment from the Taiwan Strait. Shaded area on the left shows relatively coarse sediment ($\phi < 5.5$) and shaded area to the right indicates high standard deviations (> 1.7) indicative more poorly-sorted sediment.

2. Materials and methods

The 59 riverine and surficial sediment samples (Fig. 4) from the Min and Ou (mainland China) and Choshui (Taiwan) rivers (collected in August 2005) as well as sediments from Taiwan Strait (collected in May 2006) were analyzed using a CILAS Laser Particle Size Analyzer. Median grain size and standard deviation were calculated using the moment method provided by Krumbein and Pettijohn (1938). Detailed grain size processing procedure was explained in Xu et al. (2009a).

The mineralogy of 19 down-core sediment samples from northern (DE2) and middle (DE15) part of inner shelf mud wedge (purple squares in Fig. 3) was determined using X-Ray Diffraction (XRD). Particles finer than $2 \mu\text{m}$ were separated according to Stokes Law and oriented slides prepared. Identification of clay minerals was made for smectite (17 \AA), illite (10 \AA) and kaolinite + chlorite (7 \AA) on the glycolated curve. Kaolinite and chlorite were separated by relative proportions according to their area ratios of $3.57/3.54 \text{ \AA}$. Semi-quantitative analysis of peak area of clay minerals followed the calculation of intensity factors provided by Biscaye (1965).

Along the southern part of mud wedge, 14 down-core mineralogical data from two gravity cores (737 and 775, Fig. 3) were reported by You et al. (1993), using the same method for extracting the clay fraction, preparing oriented slides, and separating kaolinite from chlorite. The semi-quantitative analysis method used by You et al. (1993), however, was from Scaife and Kunze (1971), which is based on peak height rather than peak area. Harlan (1966) compared clay mineral estimates using both peak area and peak height calculations for 20 duplicate samples, and concluded that to detect the changes in the relative abundances of clay minerals comparable results will be obtained using either method. To compare semi-quantitative analysis of peak height with that of peak area is not the focus of this study, but for consistency purpose, we used the same method as Xu et al. (2009a). Moreover, as will be shown later, the major difference between Yangtze-derived and Taiwan/Min-derived sediments on the ternary diagram is the percentage of smectite. We carefully examined all XRD data published by You

et al. (1993), and found that all samples in cores 737 and 775 have detectable smectite (5–14%), indicating the definite presence of smectite in all XRD curves regardless which method was used. In fact, clay minerals in cores 737 and 775 are quite different with these from Taiwan/Min rivers in which no smectite (17 \AA) peaks are detected on XRD curves (discussed later). Even if two semi-quantitative methods produced slightly different clay mineral percentages, they should not have a significant impact on the clay mineral assemblages in this study.

Since the year 2003 a total of ~3000 km of high-resolution seismic profiles (Fig. 3) have been collected using a CHIRP sonar sub-bottom profiler (EdgeTech 0512i). All profiles were processed using EdgeTech Discover software. Four units were recognized based on their distinct acoustic features (discussed later), the units were colored using Adobe Photoshop (uncolored figures are provided as supplementary figures for comparison), and loaded into IVS Fledermaus to construct fence diagrams. An acoustic velocity of 1500 m/s was assumed to calculate water depth and sediment thickness (Chen et al., 2003).

Based on these profiles we were able to construct isopach maps of mud-wedge thickness, and by utilizing published data from hundreds of boreholes (Li et al., 2000, 2002, 2003) and additional seismic profiles (Chen and Stanley, 1993; Chen et al., 2003), we could extend the isopachs into the Yangtze delta. After UTM projection in ArcGIS3.2 and Kriging interpolation in Golden Surfer software, the volumes of isopachs were determined.

In addition to published conventional radiocarbon dates (Ye et al., 1981; Chien and Leu, 1984; Qin et al., 1987; Yu and Li, 1992; Lan et al., 1993), other AMS radiocarbon dates were obtained from molluscan shells, foraminifera and bivalve shells within sediment cores (Hori et al., 2002; Chen et al., 2003; Xiao et al., 2004; Wang et al., 2005; Xiao et al., 2005; Liu et al., 2007a; Xu et al., 2009b; Liu et al., 2010a; Wang et al., 2010a; Zheng et al., 2010). These 130 radiocarbon ages are summarized in Table 1. All radiocarbon ages were calibrated using CALIB6.0.1 (<http://intcal.qub.ac.uk/calib/>; Stuiver et al., 1998). The calibration date set was Marine 04 (Hughen et al., 2004), which includes a constant average global reservoir age of 400 yr. The calibrated ages in this study may differ with the calibrated dates in

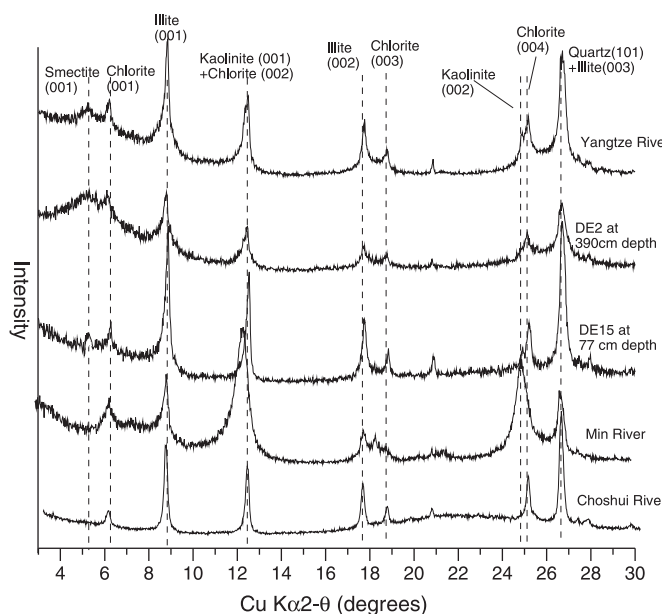


Fig. 5. Glycolated XRD curves of clay samples ($<2 \mu\text{m}$) from Yangtze, Min and Choshui rivers as well as from the bottom of cores DE2 and DE15.

original references because different data sets or versions of calibration software were used. Based on the 'law of superposition' in stratigraphy, radiocarbon dates should increase down cores; where reported dates decreased down cores, they were not used in this study. Sediment accumulation rates were calculated by dividing the difference of depth by that of age.

3. Results

3.1. Grain size

Based on median grain size, the southern part of the studied area can be classified into three distinct regions (Fig. 4 left). A muddy band extends along the inner-most part of the shelf, with a near constant median grain size of $\sim 8 \mu\text{m}$ (7 phi; Fig. 4 left). This inner shelf mud

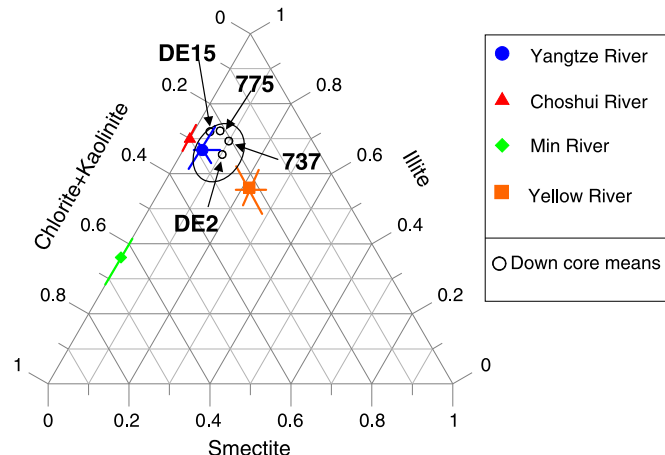


Fig. 7. Ternary diagram of clay mineralogy of Yangtze, Choshui, Min and Yellow rivers as well as the means of cores DE2, DE15, 737 and 775. (For interpretation of the references to color in this figure legend, the reader is referred to the web version of this article.)

wedge extends southward, narrowing south of the Min River mouth and reaching the southwestern corner of Taiwan Strait $\sim 24^\circ\text{N}$. The second region is seen along the middle Taiwan Strait, with a highly variable grain size from medium sand to medium silt ($<5.5 \mu\text{m}$, shaded in Fig. 4 left). The third region is seen near the northeastern part of the Taiwan Strait, covered by fresh muddy deposits in response to transient floods in western Taiwan (Milliman et al., 2007). Standard deviations in most samples are between 1 and 2 phi units, indicative of their poorly sorted nature; sediments in the middle Strait have the poorest sorting, all greater than 1.7 phi units (shaded in Fig. 4 right).

3.2. Down-core mineralogy

XRD curves show a clear similarity between Yangtze sediments and two samples from the bottom of cores DE2 and DE15 (Fig. 5), suggesting, not unreasonably, that the bulk of the sediment in the mud wedge is derived from the Yangtze River. No smectite is found in Min or Choshui river sediment, thus making an effective index to differentiate Yangtze sediment from that derived other potential sources (Fig. 5). Min sediment is unique in that it has a prominent

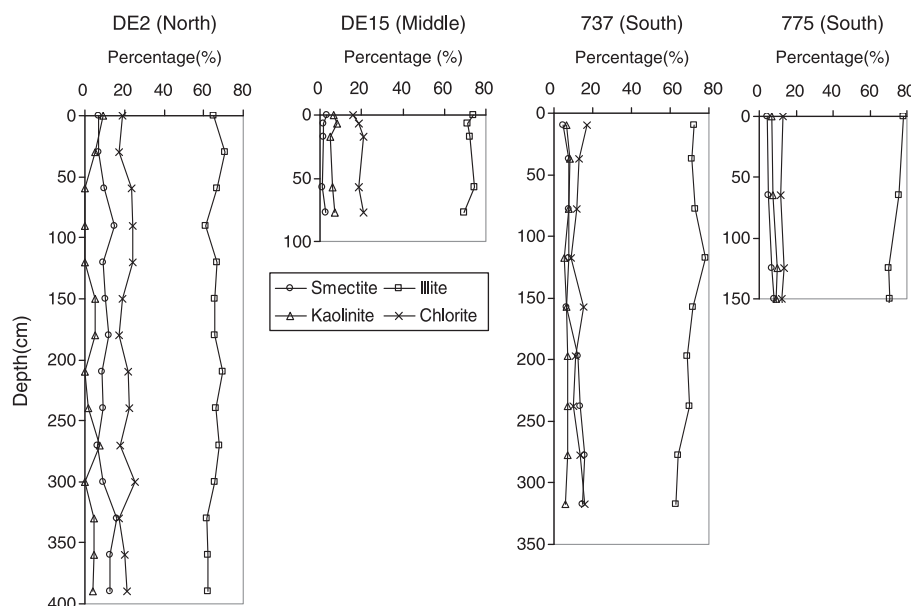


Fig. 6. Down-core variations of clay mineral percentages of cores DE2, DE15, 737 and 775.

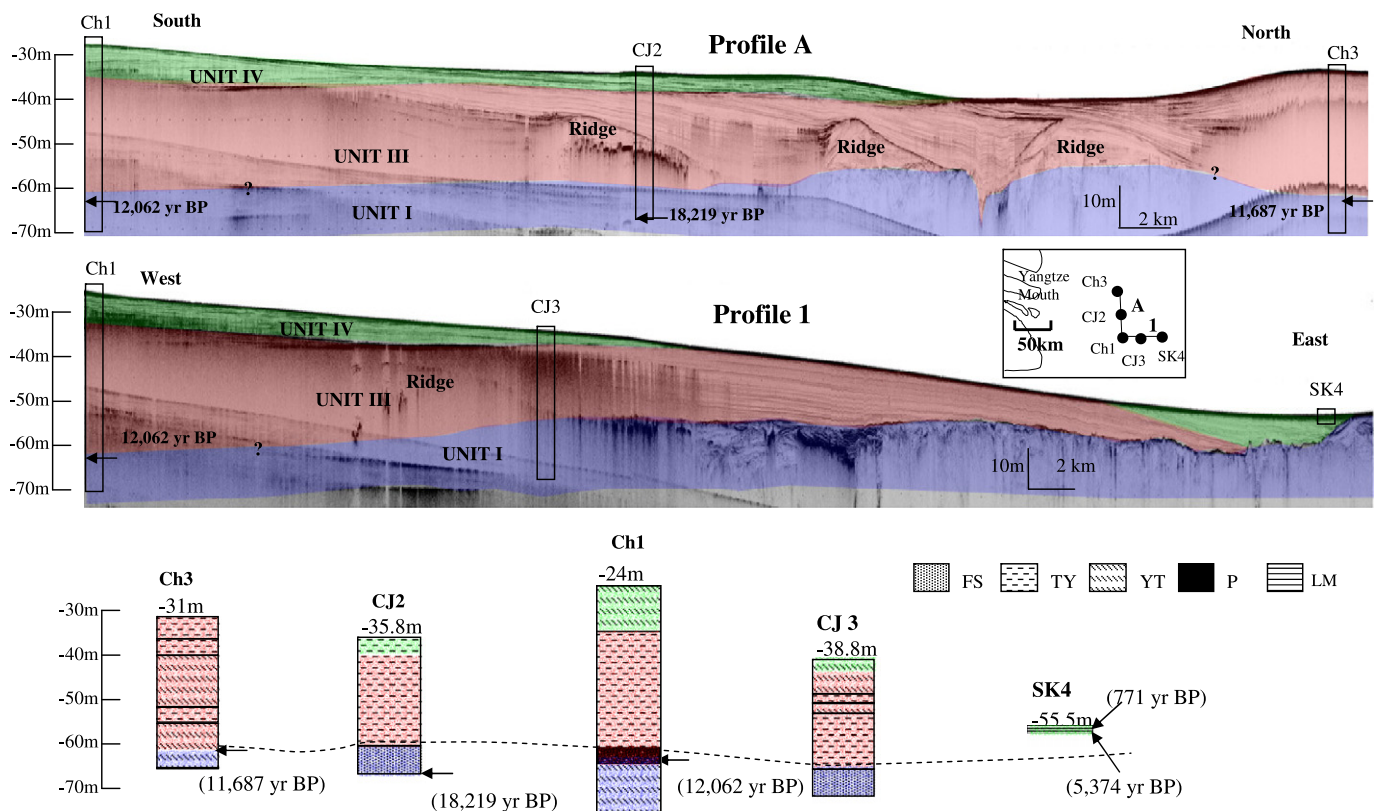
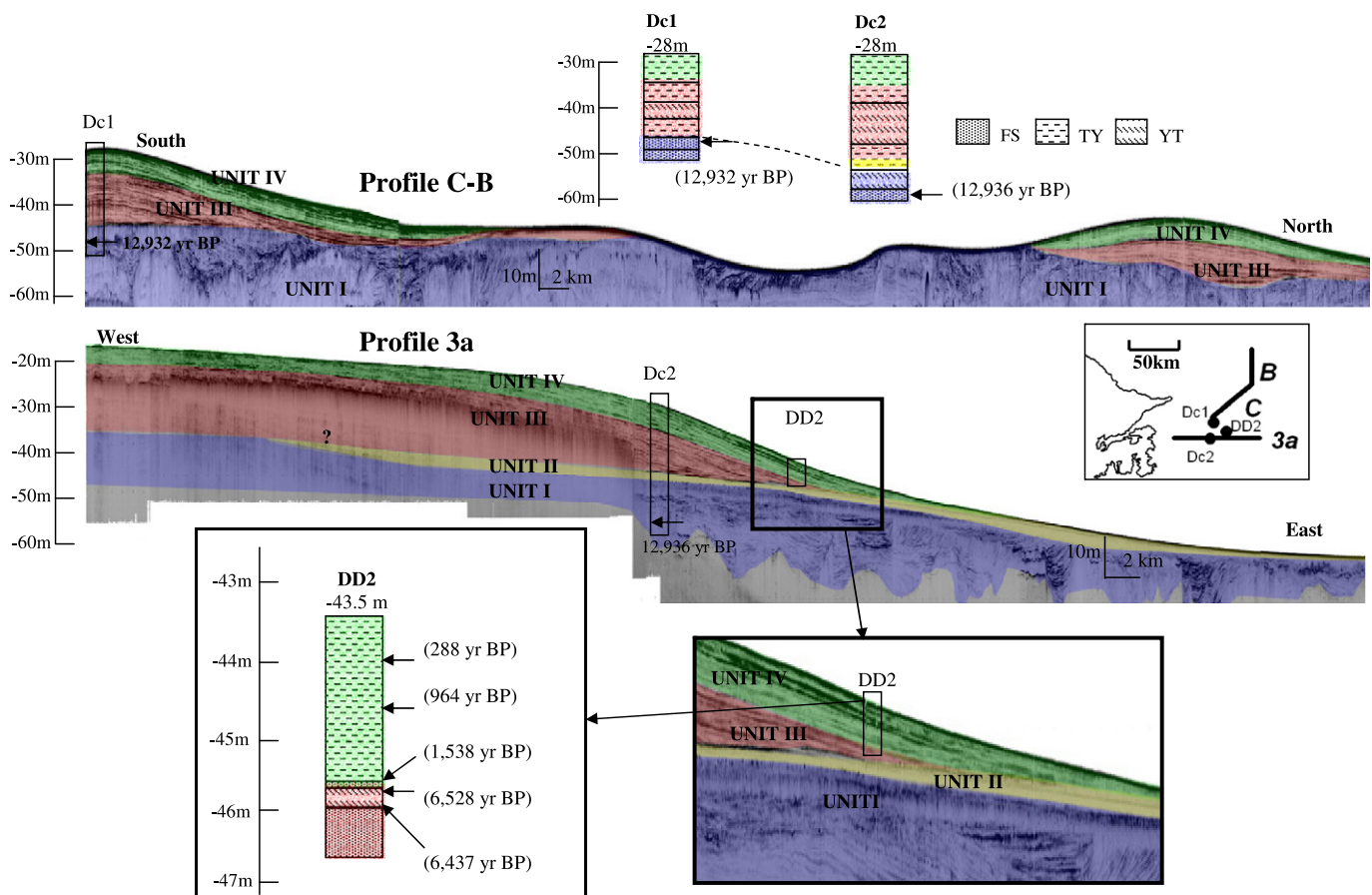


Fig. 8. CHIRP seismic profiles A and 1 near the Yangtze mouth. Units I, II, III and IV are colored blue, yellow, red and green on the profiles, respectively. Radiocarbon dates are reported in calibrated calendar year before present–1950 AD. See Fig. 3 for the locations of profiles. MS, medium sand; FS, fine sand; TY, silty clay; YT, clayey silt; P, peat; and LM, laminated mud. When biogenic gas presents, the delineations of units are based on radiocarbon dates and/or locations of nearby units in fence diagram. Question markers indicate the uncertainty of unit designations. (For interpretation of the references to color in this figure legend, the reader is referred to the web version of this article.)



kaolinite (002) peak but no chlorite (004) peak (Fig. 5). There is no dramatic change in down-core clay mineralogy in cores DE2, DE15, 737 and 775 (Fig. 6). Small variations suggest a fairly stable sediment supply along the inner shelf. A Ternary diagram indicates that sediments in these four cores are not unlike the sediment from the Yangtze River and they are distinctly from sediment of Yellow, Choshui or Min rivers (Fig. 7).

3.3. Seismic structure

From bottom up, four distinct acoustic units (I, II, III and IV), delineated as blue, yellow, red and green, respectively in Figs. 8–12) were identified in the CHIRP seismic profiles. The lower part of each profile displays a prominent subsurface reflector that truncates underlying strata at a depth of 40–90 m. Below this prominent truncation surface is unit I, which varies greatly in acoustic character from layered strata in the north and near the Yangtze subaqueous delta (profile 1, Fig. 8) to extensive flat-lying or inclined strata south of 30°N (profiles 3a, 5, and 6). Many valley fills can be identified between 30 and 60 m isobaths below the truncation (Fig. 13C), presumably formed during the last low stand of sea level.

Above the truncation surface, seen only in profiles between 30 and 26°N, i.e. south of the modern Yangtze mouth, there is a thin (<3 m), flat and acoustically transparent layer overlain by the downlap. The unit between the truncation surface and the overlying downlap is termed unit II (yellow) and lies between the 40- and 70-isobaths (Fig. 13B).

The strata downlapping onto unit II, or sometimes directly onto unit I, consist of a prograding mud wedge that can be divided into two units. The lower part (relatively dipping and transparent, e.g., profile 5 in Fig. 10) is termed unit III (red), and the more flat and opaque upper part is unit IV (green). Units III and IV are separated either by angular unconformities (profiles A, 1 and 5) or by acoustically opaque strata (profiles C-B, 3a, tw1 and tw2) (Figs. 8–12). Units III and IV are seen from Yangtze mouth to the Taiwan Strait, but unit III (landward of 70 m isobath) occupies a larger area than unit IV (landward of 50 m isobath). In the northern part of the mud wedge, units III and IV prograde eastward and northward (Fig. 8), but in the south they mainly prograde southeastward (Fig. 10).

Biogenic gas occurs widely along the inner-most part of the ECS between 25 and 32°N, in the inner-most part of the shelf where the total thickness of units III and IV is greater than ~10 m (Figs. 8–12). In addition, it is distributed from blue unit I up to red unit III in most profiles, but occasionally can penetrate upward into green unit IV. Gas in some profiles displays a continuous “dome-like” shape (e.g., profile 3a), but in others it is discontinuous (profiles 1 and 6). No gas is seen off Taiwanese (purple) deposits (Figs. 11 and 12).

3.4. Radiocarbon dates

A total of 130 conventional and AMS (Accelerator Mass Spectrometry) radiocarbon dates were used to determine the ages of four acoustic units (Fig. 8–11; Table 1). Blue unit I is the oldest, with some ages around 30 kyr BP (1000 s of year Before Present, where Present = 1950 A.D.) in the Taiwan Strait, but most ages are younger than 20 kyr BP (Table 1). Age of the lowest portions of yellow unit II depends on location of mud wedge and timing of rapid transgressions (discussed in Section 4.2). The upper part of unit II, however, has an age of ~11 kyr BP, as indicated by the dates in cores Ch1, Ch3, EC2005 and MD06-3039/3040. Sediments above Unit II are thus younger than 11 kyr BP. ¹⁴C dates at the top of Unit III range from 3.28 to 4.3 kyr BP (cores MD06-3039/3040 and EC2005, respectively), significantly

older than the bottom of Unit IV (1.29, 1.36, 1.54, and 1.80 kyr BP in cores MD06-3039/3040, PC6, DD2, and EC2005, respectively). Since there are low accumulation rates or even truncations between units III and IV (discussed in Section 4.4), we infer that the beginning of formation of unit IV was about 2 kyr BP. Thus the periods of units III and IV are 11–2 and <2 kyr BP, respectively.

4. Discussion

4.1. Mud wedge provenance

The inner-shelf mud wedge has a typical median grain size of 8 µm (7 phi, Fig. 4 left), extending from the Yangtze mouth 1000 km southward to the southwestern corner of the Taiwan Strait. Probably due to the declining strength of Yangtze dispersal system and the blocking of the Taiwan Warm Current (Fig. 1), the mud wedge narrows south of the Min River mouth and diminishes ~24°N (Fig. 4 left). Standard deviation describes the sorting of sediment, which in turn is a measure of the range of grain sizes and the magnitude of the spread or scatter of grain size distribution (Boggs, 2006). Greater standard deviations tend to indicate either highly-variable energy of depositional environment or, more likely in this case, a mixture of multiple sources. The high-standard-deviation area (shaded in Fig. 4 right) may reflect the mixing of muddy Yangtze sediment transported from the north (Xu et al., 2009a) and sand–silt-dominated Taiwanese sediment from the south (Liu et al., 2008a).

Surficial XRD mineralogical data indicate that modern Yangtze-derived clay is illite-dominated (~70%), with lesser amounts of kaolinite and chlorite as well as a small amount of smectite (5%) (Xu et al., 2009a). Down-core mineralogical data from the northern (Core DE2) and middle (Core DE15) mud wedge, together with published mineral data of cores 737 and 775 in the southern mud wedge (You et al., 1993), indicate that most down-core clays are also illite-dominated (70%), with little variation from top to bottom (Fig. 6), suggesting that the sediments in the in northern, middle and southern mud wedge are primarily Yangtze-derived (Fig. 7).

In the Taiwan Strait, a thick sequence (purple in Figs. 11 and 12) progrades northward from a subaqueous delta offshore the Choshui River mouth, and mixes with Yangtze distal mud wedge between 25 and 26°N (Fig. 12D). This deltaic deposit is silt–sand-dominated, up to 50 m thick, and has a mean annual accumulation of 60 Mt/yr (Liu et al., 2008a). In contrast to the Yangtze mud wedge, this deltaic deposit contains no biogenic gas nor do the clays contain smectite, and the sequence progrades northwestward. All these observations suggest the derivation from Taiwanese rivers and northwestward transport by Taiwan Warm Currents (Fig. 12D). The above data of grain size (Fig. 4), mineralogy (Fig. 7) and progradation direction of seismic profiles (Fig. 12), have allowed us to redefine the Yangtze- and Taiwan-derived isopachs (Liu et al., 2007a, 2008a) in Fig. 13A.

4.2. Sea-level changes and mud wedge formation

Because of the large sediment supply and the wide and gentle shelf gradient, formation of inner ECS mud wedge has been particularly sensitive to sea-level change. Since the Last Glacial Maximum (~18 kyr BP in ¹⁴C age and ~21 kyr BP in calibrated age; Wang and Sun, 1994), there have been six periods of rapid sea level rise (Fig. 14), in two of which sea level rose 20 m (~96 to ~76 m, 14.3–14.0 kyr B: MWP-1A) and 13 m (~58 to ~45 m, 11.5–11.2 kyr BP: MWP-1B), respectively, each rise occurring in about 300 yr (Fairbanks, 1989; Bard et al., 1990; Liu and Milliman, 2004). Sea level reached its highest

Fig. 9. CHIRP seismic profiles 3a and C-B. See Fig. 8 caption for sediment, color, and unit definitions. See Fig. 3 for the locations of profiles. Note that very low sediment accumulation between 1538 and 6528 yr BP in core DD2. When biogenic gas presents, the delineations of units are based on radiocarbon dates and/or locations of nearby units in fence diagram. (For interpretation of the references to color in this figure legend, the reader is referred to the web version of this article.)

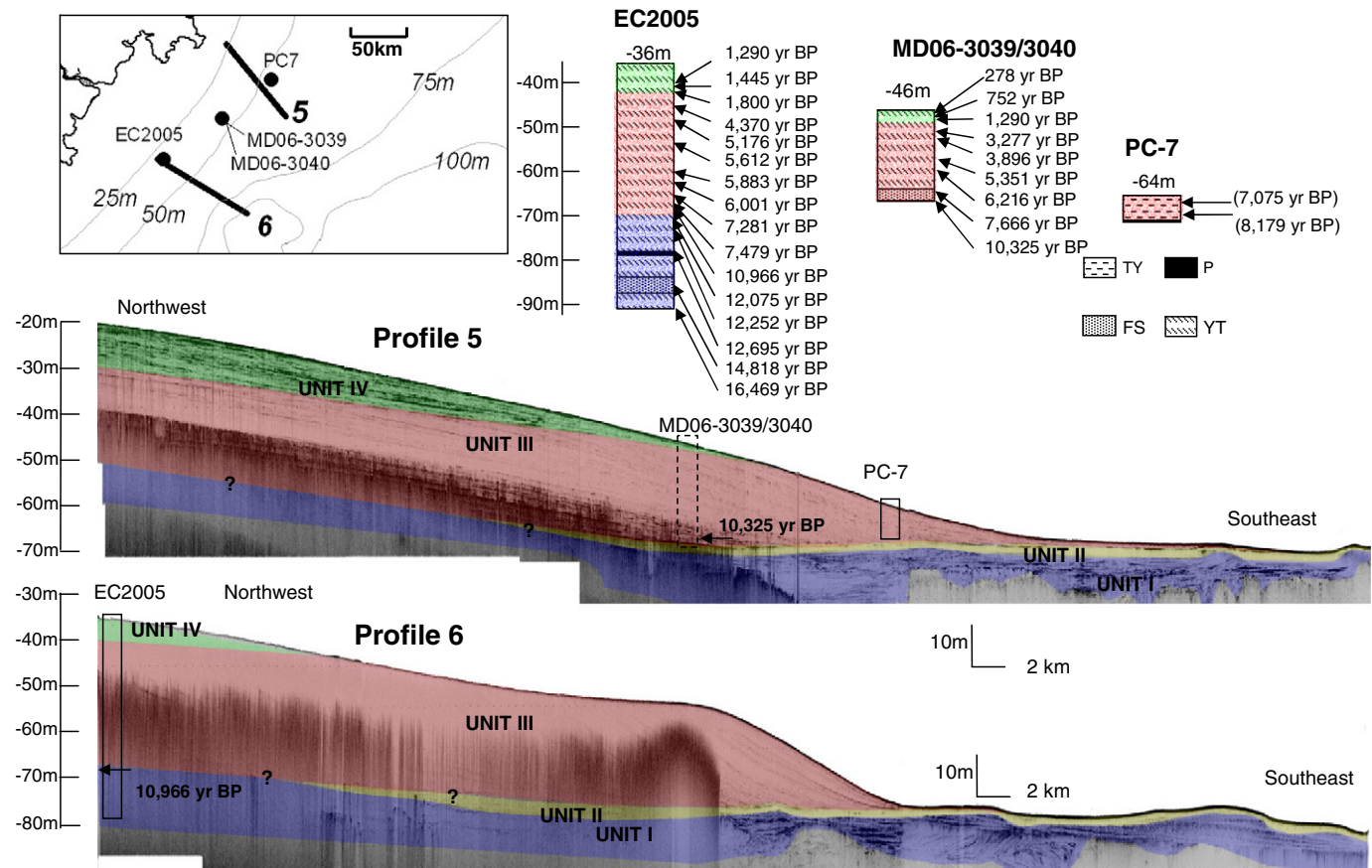


Fig. 10. CHIRP seismic profiles 5 and 6 near the southern Yangtze depocenter. See Fig. 8 caption for sediment, color, and unit definitions. See Fig. 3 for the locations of profiles. When biogenic gas presents, the delineations of units are based on radiocarbon dates and/or locations of nearby units in fence diagram. Core MD06-3039/3040 is located in a 46-m water depth, and is far from profile 5. But for comparison purpose, core MD06-3039/3040 is shown as a dashed bar at a water depth of 46 m on profile 5. Acoustically no obvious truncation is found on top of profile 6, but units III and IV were interpreted based in the radiocarbon ages. (For interpretation of the references to color in this figure legend, the reader is referred to the web version of this article.)

level at +3 m around 7 kyr BP and since then has slowly regressed to its present level (Chen and Stanley, 1998).

Considering its wide depth range, −40 m to −90 m in most profiles (Figs. 8–11), unit II is assumed to have formed during MWP-1A and/or 1B, i.e. between 14.3 and 11.2 kyr BP. During these two rapid transgressions, unit I was swept and truncated by paleo-tidal currents that may have been stronger than modern ones (Uehara et al., 2002; Uehara and Saito, 2003), and the Yangtze mouth retreated rapidly northwestward. After these two transgressions, the wide southern inner shelf was far from the Yangtze mouth and thereby sediment-starved, only a small amount of fine sediment reaching south of 30°N. North of 30°N and near the paleo-Yangtze mouth, however, Yangtze sediment downlapped directly onto unit I due to the close proximity to the river. South of 26°N, little sediment seems to have been preserved, either because it was too far from the sediment source or because the paleo-China Coastal Current did not extend that far.

After MWP-1B (~11 kyr BP), when sea level had risen to ~−45 m, the Yangtze River began to develop its mud wedge on the inner shelf and the southern depocenter began to receive a continuous sediment supply, as seen in cores EC2005 and MD06-3039/3040 (Fig. 10). Sediment accumulation between 11 and 7 kyr BP was about 8 and 6 m at the middle or bottom of cores EC2005 and MD06-3039/3040, respectively (Figs. 10 and 14). Although Liu et al. (2007a) suggested that between 11 and 7 kyr BP the Yangtze River transported sediment into the southern Yellow Sea, evidence from two cores of EC2005 and MD06-3039/3040 shows continuous sedimentation to the south during this period. We therefore infer that the Yangtze River has continued transporting sediment southward since 11 kyr BP.

Around 7 kyr BP, when sea level had risen to and slightly above its present level (Fig. 14), the Yangtze mouth retreated northwestward close to its modern location, or even farther inland. As sea level became stabilized (Chen and Stanley, 1998; Hori et al., 2001b), the China Coastal Current became a more permanent feature by which sediments could be resuspended and transported southward toward the Taiwan Strait.

4.3. Lithology and stratigraphic interpretation

Of the units defined in Section 3.3, Unit I lies below the truncation surface. Gravity cores indicate that this truncation tends to be a fine-sand layer (bottom of CJ2, CJ3, Dc1, Dc2 and MD06-3039/3040 in Figs. 8–10). Comparing published seismic profiles from Yellow Sea (Liu et al., 2002, 2004), Yangtze subaqueous delta (Chen and Stanley, 1993; Chen et al., 2003), and inner ECS shelf (Liu et al., 2007a), we assume that this reflector represents a transgressive surface separating underlying a sandy late-Pleistocene unit I (blue) from the overlying younger units.

Unit II is acoustically transparent, probably reflecting fine texture of its sediment. Cores Dc2 and EC2005, which penetrate through unit II (Figs. 9 and 10), have relatively little grain size variation, promoting this unit's acoustic reflectivity. Since unit II was formed during rapid sea level transgression between 14.3 and 11.2 kyr BP (including MWP-1A and 1B), it should be considered as a transgressive systems tract (TST).

Units III and IV represent a prograding mud wedge, and gravity and box cores indicate they are dominated by muddy sediment: silty

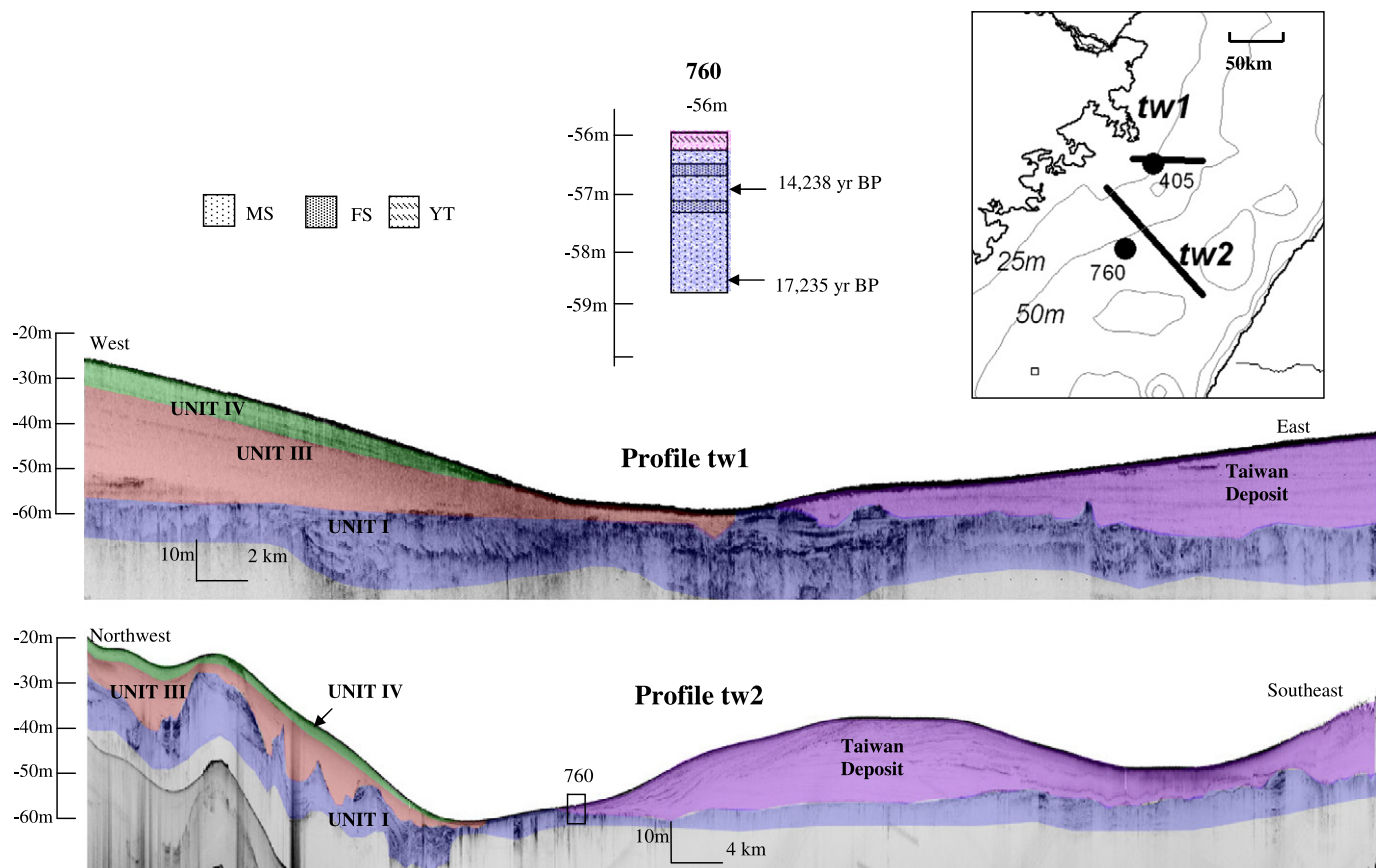


Fig. 11. CHIRP seismic profiles tw1 and tw2 in the northern Taiwan Strait. See Fig. 8 caption for sediment, color, and unit definitions. Taiwanese deposits are in purple. See Fig. 3 for the locations of profiles. (For interpretation of the references to color in this figure legend, the reader is referred to the web version of this article.)

clay or clayey silt (Figs. 8–11). The distinct feature of unit III is the downlap, i.e. initially inclined strata terminating downdip against initially horizontal or inclined strata (Mitchum et al., 1977; Boggs, 2006). Near the Yangtze subaqueous delta, seismic profiles show several ridge-like acoustic units in unit III respectively (Fig. 8), which have been interpreted as 'Early Holocene mud ridges' by Chen et al. (2003). Similar relict sand ridges (Liu et al., 1998, 2007b) are widely distributed farther southeastward to the middle shelf (Fig. 13 C), trending approximately parallel to the direction of tidal flow (Chen et al., 2003).

Unit III was formed between 11 and 2 kyr BP, but because sea level reached the highest level at 7 kyr BP, designation of system tract of unit III becomes challenging. Transgression and regression are accompanied with progradation and retrogradation of shorelines, respectively. Due to localized high sediment supply, Yangtze subaqueous delta might continue to prograde during the transgression of sea level in 11–7 kyr BP (Catuneanu, 2006). Thus theoretically the lower part (11–7 kyr BP) of unit III can also be regarded as a part of TST, but distinctly different from unit II. The upper part (7–2 kyr BP) of units III and IV can be defined as early and late highstand systems tract (HST), respectively.

4.4. Episodic accumulation

^{14}C -derived dates from the various cores suggest that sediment accumulation rates during the past 14 kyr have varied from 20 to <1 m/kyr (Fig. 15). There appear to have two high-accumulation-rate periods, 5–8 kyr BP and 0–2 kyr BP, and one low-accumulation-rate period, 2–5 kyr BP, (Fig. 15). This episodic deposition suggests the complex nature of the Yangtze sediment dispersal system.

Accumulation rates in the southern depocenter (*sink*) are controlled by supply from Yangtze drainage basin (*source*), accumulation in the northern Yangtze depocenter (Yangtze delta, *trapping*), as well as circulation and strength of currents in the inner shelf (*transport*). Assuming no dramatic change in currents, increased accumulated rates at both northern and southern depocenters suggest an increased Yangtze sediment flux. If there is no change in Yangtze flux, decreased accumulation at the northern depocenter and increased accumulation at the southern depocenter probably reflect increased transport by coastal currents.

Comparing northern with southern depocenter (Fig. 14), we find that both depocenters started to develop as early as ~13 kyr BP. Rapid sea-level rise during MWP-1A and 1B provided plenty of accommodation space for the southern depocenter, leading to continuous deposition there. Based on various geological data, including lake levels, pollen profiles, and loess/paleosol records, An et al. (2000) concluded that East Asian summer monsoon precipitation in the middle and lower reaches of the Yangtze River reached its Holocene maximum about 5–7 kyr BP. Because Yangtze water and sediment discharge are controlled by both climatic and anthropogenic forcings (Xu et al., 2006, 2007, 2010; Xu and Milliman, 2009), high accumulation rates 5–8 kyr BP in the southern depocenter are probably related to high precipitation in the Yangtze drainage basin and thus high discharge to the ECS.

Low (5–2 kyr BP) and high (2–0 kyr BP) accumulation periods match well with shoreline changes based on Yangtze Delta chenier record (Chen, 1998). Yangtze seaward progradation rate was 38 m/yr in 6–2 kyr BP, but increased to 80 m/yr after 2 kyr BP, primarily in response to increased human activities (Hori et al., 2001b), leading to increased erosion. Pollen studies also have revealed remarkable changes in arboreal and herbaceous vegetation after 1.3 kyr BP,

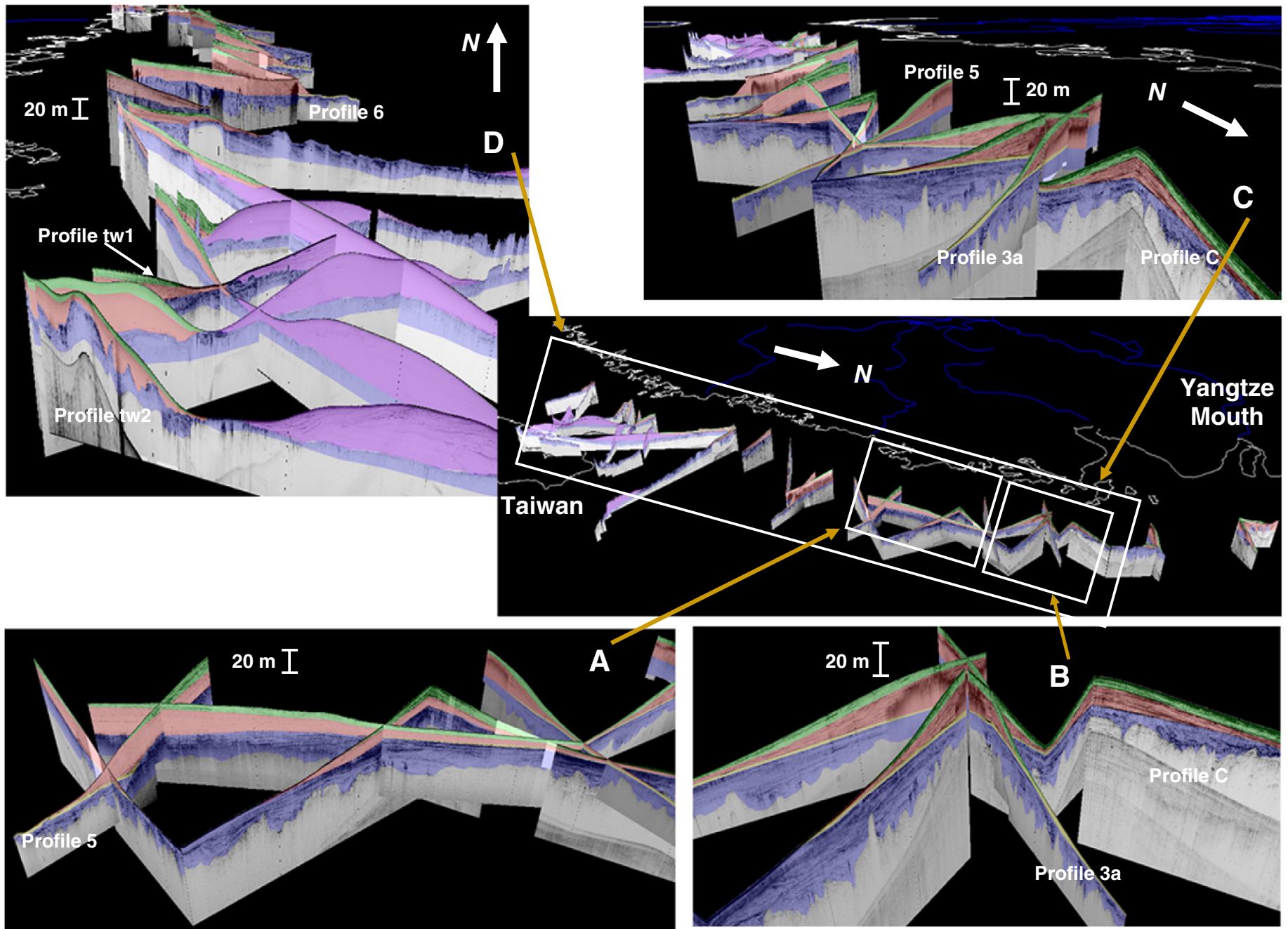


Fig. 12. Fence diagram of CHIRP seismic profiles. Unit I (blue), II (yellow), III (red, 2–11 kyr BP) and IV (green, 0–2 kyr BP) are colored on the profiles. Northward prograding Taiwan deposit is in purple, derived mainly from the western Taiwanese rivers. Note that Yangtze mud wedge overlaps with Taiwan deposit in Fig. 12D. Uncolored profiles are provided as supplementary online materials.

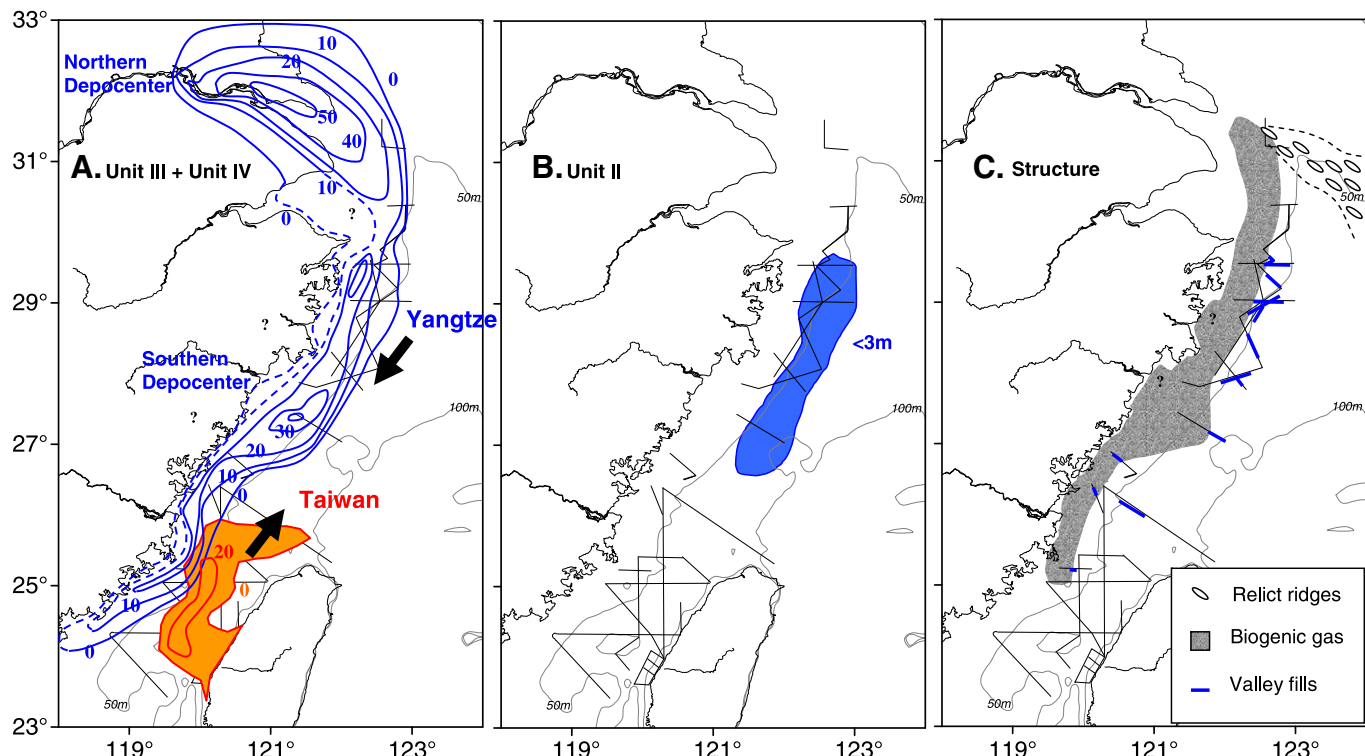


Fig. 13. A. Isopach (in m) of post-MWP-1B Yangtze mud wedge (units III and IV), modified after Fig. 12 in Liu et al. (2007a) and Fig. 12 in Liu et al. (2008a); B. Location and thickness (in m) of unit II; C. Sedimentary features, including biogenic gas, valley fills and relict ridges. 50- and 100-m isobaths are show in italic on all panels. (For interpretation of the references to color in this figure legend, the reader is referred to the web version of this article.)

reflecting intensive human activities such as rice cultivation and deforestation in the Yangtze basin (Yi et al., 2003).

One of the most intriguing aspects of the post-MWP-1B mud wedge is the truncation or low accumulation between unit III and IV, around 2–5 kyr BP. At first glance this truncation may seem related to short-term sea-level regression, but sea level was fairly stable during

this time (Fig. 14). Moreover, if there were regression-related erosion, this truncation should be seen in all the profiles. The unconformities seen near the Yangtze mouth and southern depocenter might also be caused by low river discharge or other processes, as explained below.

Near the Yangtze mouth, the truncation is found at 30 m depth in profiles 1 and A (Fig. 8). On a closer inspection, in profile A there are actually a series of truncations, one in unit III and several in unit IV. These truncations might be related to frequent hydrodynamic changes near the Yangtze River mouth. The Yangtze delta has been prograding gradually during the Holocene, and as such its apex has shifted ~250 km southeastward (Li et al., 2002). The passages and channels in Yangtze estuary thus have kept changing their locations, which presumably would have changed estuarine circulation and sediment dispersal patterns, thus causing erosion or reworking of older sediment.

The truncations at 40–60 m depth in profiles 5 and 6 at southern depocenter (Fig. 10), however, are probably related to changes in the coastal currents. Following the re-intensification of the southwest monsoon around 11 kyr BP, the climate in southern Asia became increasingly warm and wet (Thompson et al., 1989; Gasse et al., 1991). Palynological studies of long boreholes in the Yangtze delta have revealed that the climate switched from warm/wet to cool/dry conditions and back several times (Yi et al., 2003), particularly during late Holocene. Related to this may be changes in the path and velocity of coastal currents, not unlike some deep sea drift deposits (Tucholke et al., 1985; McCave and Tucholke, 1986; Tucholke, 2002). Although direct evidence is hard to collect, the slight truncations between unit III and IV might be related to intensified Taiwan Warm Current and China Coastal Current, or east-west shifting of the axes of currents.

4.5. Comparison between long- and short-term accumulation rates

Based on ^{210}Pb geochronological data derived from gravity and box cores (DeMaster et al., 1985; Alexander et al., 1991; Chen, 1995;

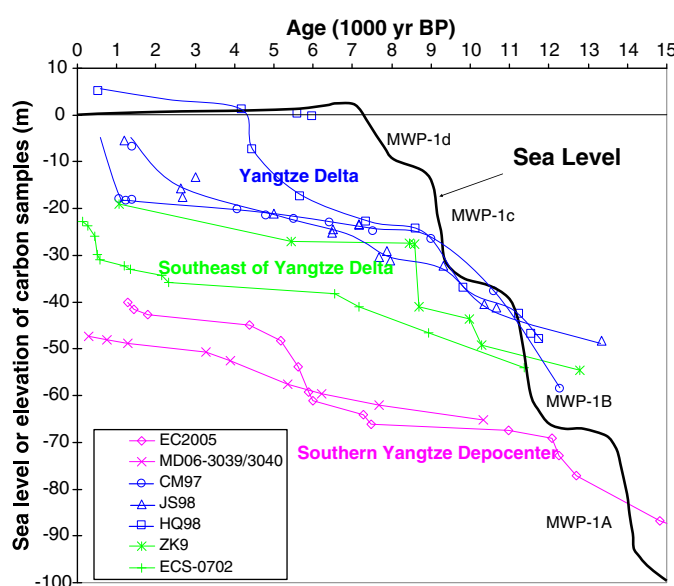


Fig. 14. Sea level variations since 15,000 yr BP (from Liu et al., 2004), as well as radiocarbon dates derived from three boreholes in the Yangtze delta [CM97, JS98 and HQ98 from Hori et al. (2002)], two cores southeast of the Yangtze Delta [ZK9 from Wang et al. (2010a)] and ECS-0702 from Liu et al. (2010a)], and two giant piston cores in the southern depocenter [EC2005 from Xu et al. (2009b); MD06-3039/3040 from Zheng (2010)]. (For interpretation of the references to color in this figure legend, the reader is referred to the web version of this article.)

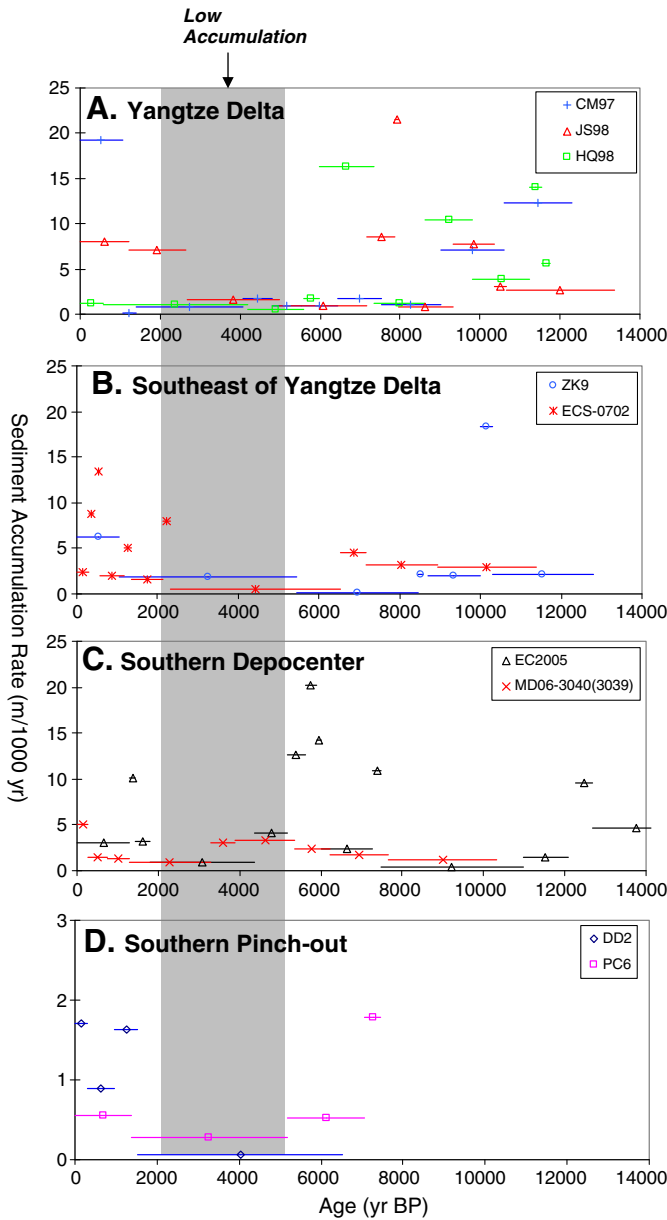


Fig. 15. Sediment accumulation rates at the Yangtze delta, southeast of the Yangtze delta, southern depocenter, and near-pinch-out site during the past 14 kyr. See Fig. 3 for the locations of cores. Note that between 2 and ~5 kyr BP the accumulation rates were low. (For interpretation of the references to color in this figure legend, the reader is referred to the web version of this article.)

Chung and Chang, 1995; Huh and Su, 1999; Xia et al., 1999, 2004; Su and Huh, 2002; Oguri et al., 2003; Liu et al., 2006), short term (100-yr time scale) sediment accumulation rates generally exceed 1 cm/yr near the river mouth, and decrease towards Taiwan Strait (Fig. 16). Across the shelf, there also is a trend of decreasing accumulation, from 1 cm/yr in inner shelf to <0.1 cm/yr in outer shelf and Okinawa Trough (Fig. 16).

Comparing Fig. 13A with Fig. 16, we find that short term ^{210}Pb rates (1 cm/yr near the Yangtze delta) are at least 5 times greater than the long-term ^{14}C rates (only 0.2 cm/yr, ~22 m in 11 ka in Fig. 13A). Compiling a large dataset of sediment accumulation rates, Sadler (1981) reported that the discrepancy between long- and short-term accumulation rates was primarily the consequence of unsteady (may be cyclic or random) and discontinuous sedimentation. Huh and Su (1999) and Su and Huh (2002) concluded that the discrepancy can be reduced by considering the effect of sediment mixing (which overestimated sedimentation rates) and the possibility of additional

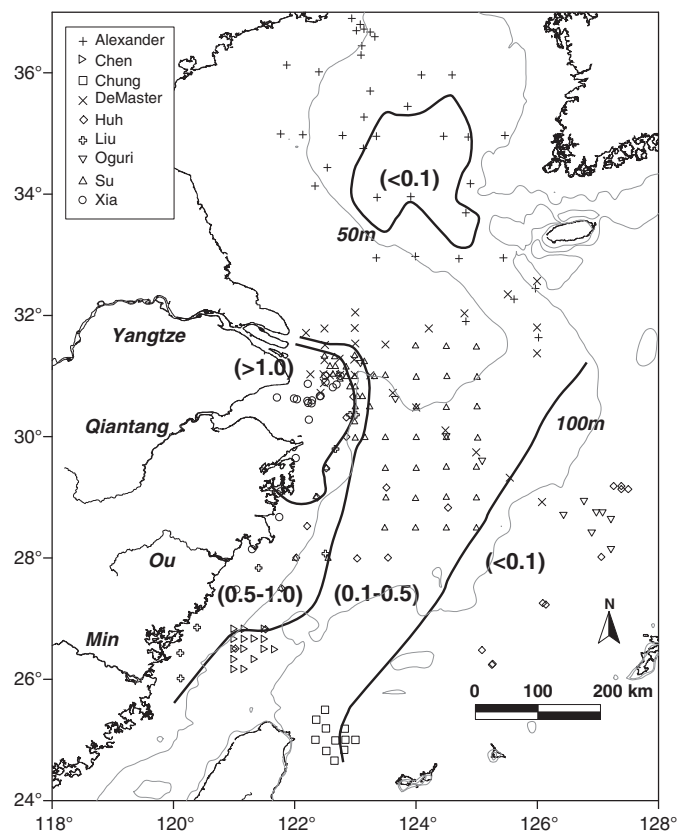


Fig. 16. Sediment accumulation rates (cm/yr) based on ^{210}Pb analyses in the East China Sea. Isobaths are shown at 50 and 100 m. Data are from DeMaster et al. (1985), Alexander et al. (1991), Chen (1995), Chung and Chang (1995), Huh and Su (1999), Xia et al. (1999, 2004), Su and Huh (2002), Oguri et al. (2003) and Liu et al. (2006).

sediment input from the Yellow River. In addition, long-term (over 100 yr) bed consolidation and de-watering processes of fresh mud and episodic sediment escaping off the mud wedge during very-rare extreme storm events cannot be captured by ^{210}Pb analysis. Despite the difference in ^{210}Pb - and ^{14}C -based accumulation rates, their overall patterns both show decreasing accumulation seaward and southward from the Yangtze estuary (Figs. 13A and 16).

4.6. Challenges in estimating Yangtze sediment budget

Extending from the Yangtze River mouth 1000 km southward into the southwestern Taiwan Strait, the elongated post-MWP-1B mud wedge (Fig. 14) thins offshore, from ~40 m at the 30-m isobath to <2 m at the 90-m isobath. Total volume of post-MWP-1B mud wedge is calculated to be $22.1 \times 10^{11} \text{ m}^3$. Knowing this volume allows us to calculate a Yangtze River sediment flux, although this calculation involves several assumptions.

- 1) We assume there has been no significant escape of Yangtze-derived sediment northward into the Yellow Sea, southward into the South China Sea, or eastward to the middle shelf of ECS since 11 kyr BP. Xu et al. (2009a) have demonstrated that northward escape is unlikely since Yellow Sea is dominated by Yellow River sediment. Liu et al. (2008b) have also shown that no significant Yangtze input into northern South China Sea. Considering the pinching-out of mud wedge (Fig. 12) and the flat, sandy nature of middle shelf (Fig. 2) eastward escape of Yangtze sediment to the middle shelf seems equally unlikely.
- 2) We assume that total input from local small mainland rivers is much smaller than the supply from the Yangtze River. Total sediment load from the Min and Ou rivers is as high as 10 Mt/yr, but a large portion of it appears to be trapped in the Min and Ou river deltas. Supporting this supposition is the fact that sediment

20 km offshore from the mouths of Min and Ou rivers is dominated by Yangtze-derived fines. Clays from the Min River, for instance, contain no smectite or chlorite (Figs. 5–7) whereas down-core mineral data from cores 737 and 775 both show significant amounts of smectite and chlorite, reflecting the dominance of Yangtze sediments.

Sediment fluxes were calculated by multiplying the volume by density, then dividing by time. An average acoustic velocity of 1500 m/s was assumed to calculate the depth of the seismic profiles, although acoustic velocity can vary from ~1400 to ~1800 m/s depending on sediment type. Limited access to coastal waters shallow than ~15 m also prevents a more accurate assessment of total sediment volume (dashed lines in Fig. 13A). Depending on the grain size and water content, dry bulk density can vary from ~0.9 to ~1.6 t/m³. Given that most of the sediment appears to be silty clay and clayey silt (Figs. 8–11), we assumed an average density of 1.2 t/m³ (Chen et al., 2003). Time error depended on radiocarbon dating methods: errors for conventional radiocarbon dating were ~500 yr and AMS dating errors were ~50 yr.

Taking into account these limitations, we calculate that sediments in units III and IV amount to 26.5×10^{11} tons, equivalent to an average annual sediment accumulation of 240 Mt/yr between 11 kyr BP and present, although keeping in mind the episodic nature of sediment flux, transport and accumulation discussed in Section 4.4. Given the uncertain input from the Yellow River when it has flowed south of the Shandong Peninsula (Liu et al., 2010a) and the small input from southern coastal rivers (Qiantang, Ou and Min), actual input from the Yangtze for the past 11 thousand years should be somewhat less than 240 Mt/yr.

5. Conclusions

- (a) Down-core clay mineralogical data indicate the mud wedge is illite-dominated, with lesser amounts of kaolinite and chlorite as well as a small amount of smectite. Clay assemblages indicate their major provenance is the Yangtze River.
- (b) Yangtze mud wedge extends along the western edge of the East China Sea and stretches from the Yangtze mouth to the southwestern Taiwan Strait, thinning from ~40 m thickness at 30-m isobath to <2 m at 80-m isobath.
- (c) From bottom up, four units have been delineated. Unit II is far from the modern Yangtze delta, and is located only between the 40- and 90-m isobaths. Units III and IV are elongated, but unit III extends eastward farther than unit IV.
- (d) During the past 11 kyr Yangtze sediment accumulation was unsteady, with two high-accumulation-rate periods (at 5–8 kyr BP and 0–2 kyr BP) and one low-accumulation-rate period (2–5 kyr BP).
- (e) High accumulation rate in 5–8 kyr BP was probably related to maximum East Asian summer monsoon precipitation in the Yangtze basin, whereas high rate in 0–2 kyr BP was formed by intensive human activities. The low-accumulation-rate period (2–5 kyr BP) was probably related to intensified Taiwan Warm Current and China Coastal Current.

Supplementary materials related to this article can be found online at doi:10.1016/j.margeo.2011.06.003.

Acknowledgements

We thank the crew of R/V Golden Star II (from Institute of Oceanology, Chinese Academy of Sciences) and R/V OR2 (from National Taiwan Ocean University) for collecting seismic profiles and marine samples used in this study. We acknowledge Drs. Peng Huang (IOCAS), Zhongyuan Chen (East China Normal University), as well as Saulwood Lin (National Taiwan University) for facilitating the fieldwork and providing some of the sediment samples used in this study. We also are grateful to Dr. Brian Tuckholke (WHOI), anonymous reviewers, and the editor David Piper, who provided

valuable comments and suggestions. This project was partly supported by National Basic Research Program of China (2010CB951202), National Science Foundation of China (4057603), and Knowledge Innovation Program of Chinese Academy of Sciences. Dr. Milliman received support from the US National Science Foundation and the US Office of Naval Research.

References

- Alexander, C.R., DeMaster, D.J., Nittrouer, C.A., 1991. Sediment accumulation in a modern epicontinental-shelf setting: The Yellow Sea. *Marine Geology* 98 (1), 51–72.
- An, Z., Porter, S.C., Kutzbach, J.E., Xihao, W., Suming, W., Xiaodong, L., Xiaoqiang, L., Weijian, Z., 2000. Asynchronous Holocene optimum of the East Asian monsoon. *Quaternary Science Reviews* 19 (8), 743–762.
- Bard, E., Hamelin, B., Fairbanks, R.G., 1990. U-Th ages obtained by mass spectrometry in corals from Barbados: sea level during the past 130,000 years. *Nature* 346, 456–458.
- Berne, S., Vagner, P., Guichard, F., Lercolais, G., Liu, Z., Trentesaux, A., Yin, P., Yi, H.I., 2002. Pleistocene forced regressions and tidal sand ridges in the East China Sea. *Marine Geology* 188 (3–4), 293–315.
- Biscaye, P.E., 1965. Mineralogy and sedimentation of recent deep-sea clay in the Atlantic Ocean and adjacent seas and oceans. *Geological Society of America Bulletin* 76 (7), 803–831.
- Boogs, S., 2006. Principles of sedimentology and stratigraphy, 4th edition. Prentice Hall, p. 688.
- Catuneanu, O., 2006. Principles of sequence stratigraphy. Elsevier Press, p. 386.
- Chen, S.K., 1995. Sediment accumulation rates and organic carbon deposition in the East China Sea continental margin sediments. MS Thesis, National Taiwan University, Taipei, Taiwan, 80 pp.
- Chen, X., 1998. Changjiang (Yangtze) River Delta, China. *Journal of Coastal Research* 14 (3), 838–858.
- Chen, Z., Stanley, D.J., 1993. Yangtze delta, eastern China: 2. Late Quaternary subsidence and deformation. *Marine Geology* 112 (1–4), 13–21.
- Chen, Z., Stanley, D.J., 1998. Sea-level rise on eastern China's Yangtze delta. *Journal of Coastal Research* 14 (1), 360–366.
- Chen, Z.Y., Song, B.P., Wang, Z.H., Cai, Y.L., 2000. Late Quaternary evolution of the subaqueous Yangtze Delta, China: Sedimentation, stratigraphy, palynology, and deformation. *Marine Geology* 162, 423–441.
- Chen, Z., Saito, Y., Hori, K., Zhao, Y., Kitamura, A., 2003. Early Holocene mud-ridge formation in the Yangtze offshore, China: A tidal-controlled estuarine pattern and sea-level implications. *Marine Geology* 198 (3–4), 245–257.
- Chien, M.P., Leu, T.C., 1984. Paleomagnetic inclination variations in Taiwan Strait sediments after Holocene transgression. *Journal of Oceanography Taiwanica* 15, 53–70.
- Chung, Y., Chang, W.C., 1995. Pb-210 fluxes and sedimentation rates on the lower continental slope between Taiwan and the South Okinawa Trough. *Continental Shelf Research* 15 (2–3), 149–164.
- DeMaster, D.J., McKee, B.A., Nittrouer, C.A., Jiangchu, Q., Guodong, C., 1985. Rates of sediment accumulation and particle reworking based on radiochemical measurements from continental shelf deposits in the East China Sea. *Continental Shelf Research* 4 (1–2), 143–158.
- Fairbanks, R.G., 1989. Glacio-eustatic sea level record 0–17,000 years before present: Influence of glacial melting rates on Younger Dryas event and deep ocean circulation. *Nature* 342 (7), 637–642.
- Gasse, F., Arnold, M., Fontes, J.C., Fort, M., Gibert, E., Huc, A., Bingyan, L., Yuanfang, L., Qing, L., Melieres, F., Campo, E.V., Fubao, W., Qingsong, Z., 1991. A 13,000-year climate record from western Tibet. *Nature* 353 (6346), 742–745.
- Harlan, R.W., 1966. A clay mineral study of recent and Pleistocene sediments from the Sigsbee Deep, Gulf of Mexico. Thesis, Texas A & M University, College Station, Texas, 140 pp.
- Hori, K., Saito, Y., Zhao, Q., Cheng, X., Wang, P., Sato, Y., Li, C., 2001a. Sedimentary facies and Holocene progradation rates of the Changjiang (Yangtze) delta, China. *Geomorphology* 41 (2–3), 233–248.
- Hori, K., Saito, Y., Zhao, Q., Cheng, X., Wang, P., Sato, Y., Li, C., 2001b. Sedimentary facies of the tide-dominated paleo-Changjiang (Yangtze) estuary during the last transgression. *Marine Geology* 177 (3–4), 331–351.
- Hori, K., Saito, Y., Wang, P., Zhao, Q., 2002. Evolution of the coastal depositional systems of the Changjiang (Yangtze) River in response to Late Pleistocene–Holocene sea-level changes. *Journal of Sedimentary Research* 72, 884–897.
- Hu, D., Saito, Y., Kempe, S., 1998. Sediment and nutrient transport to the coastal zone. In: Galloway, James N., Melillo, Jerry M. (Eds.), *Asian change in the context of global climate change: impact of natural and anthropogenic changes in Asia on global biogeochemical cycles*. : IGBP Book Series, 3. Cambridge University Press, pp. 245–270.
- Huang, H., Tang, B., Yang, W., Yuan, Y., Zhou, C., Jiu, Y., Yang, Q., 1996. *Sedimentary geology of the Yangtze River Delta*. China Geology Press, Beijing, 244 pp.
- Hughen, K.A., Baillie, M.G.L., Bard, E., Beck, J.W., Bertrand, C.J.H., Blackwell, P.G., Buck, C.E., Burr, G.S., Cutler, K.B., Damon, P.E., Edwards, R.L., Fairbanks, R.G., Friedrich, M., Guililderson, T.P., Kromer, B., McCormac, G., Manning, S., Ramsey, C.B., Reimer, P.J., Reimer, R.W., Remmelle, S., Sounthor, J.R., Stuiver, M., Talamo, S., Taylor, F.W., vander Plicht, J., Weyhenmeyer, C.E., 2004. *Marine04: Marine radiocarbon age calibration, 26–0 ka BP*. *Radiocarbon* 46, 1059–1086.
- Huh, C.-A., Su, C.-C., 1999. Sedimentation dynamics in the East China Sea elucidated from ²¹⁰Pb, ¹³⁷Cs and ^{239,240}Pu. *Marine Geology* 160 (1–2), 183–196.

- Krumbein, W.C., Pettijohn, F.J., 1938. Manual of sedimentary petrography. Appleton-Century Crofts, New York. 549 pp.
- Laj, C., the on-board scientific party, 2006. MD155-Marco Polo 2 IMAGES XIV cruise report, des rapports de campagnes à la mer, IPEV, ref OCE/2006/06.
- Lan, D.Z., Zhang, W.L., Chen, C.H., Xie, Z.T., Yu, Y.F., Cai, F., 1993. Transgressions and the sea-level changes of the western Taiwan Striat since the Late Pleistocene. *Acta Oceanologica Sinica* 12 (4), 617–627.
- Li, C., Chen, Q., Zhang, J., Yang, S., Fan, D., 2000. Stratigraphy and paleoenvironmental changes in the Yangtze Delta during the Late Quaternary. *Journal of Asian Earth Sciences* 18 (4), 453–469.
- Li, C., Wang, P., Sun, H., Zhang, J., Fan, D., Deng, B., 2002. Late Quaternary incised-valley fill of the Yangtze delta (China): Its stratigraphic framework and evolution. *Sedimentary Geology* 152 (1–2), 133–158.
- Li, B.H., Li, C.X., Shen, H.T., 2003. A preliminary study on sediment flux in the Changjiang Delta during the postglacial period. *Science in China Series D* 46 (7), 743–752.
- Li, Z., Song, B., Saito, Y., Li, J., Li, Z., Lu, A.Q., 2009. Sedimentary facies and geochemical characteristics of Jiangdou Core JD01 from the upper delta plain of Changjiang (Yangtze) delta. In: Amorosi, A. (Ed.), Proceedings of the 27th IAS meeting of sedimentologists. Medimond, Italy, pp. 55–63.
- Liao, H.-R., Yu, H.-S., Su, C.-C., 2008. Morphology and sedimentation of sand bodies in the tidal shelf sea of eastern Taiwan Strait. *Marine Geology* 248 (3–4), 161–178.
- Lin, C.-M., Zhuo, H.-C., Gao, S., 2005. Sedimentary facies and evolution in the Qiantang River incised valley, eastern China. *Marine Geology* 219, 235–259.
- Liu, J.P., Milliman, J.D., 2004. Reconsidering melt-water pulses 1A and 1B: Global impacts of rapid sea-level rise. *Journal of Ocean University of China* 3 (2), 183–190.
- Liu, Z.X., Xia, D., Berne, S., Wang, K., Marsset, T., Tang, Y., Bourillet, J.F., 1998. Tidal deposition systems of China's continental shelf, with special reference to the eastern Bohai Sea. *Marine Geology* 145 (3–4), 225–253.
- Liu, Z.X., Berne, S., Saito, Y., Lericolais, G., Marsset, T., 2000. Quaternary seismic stratigraphy and paleoenvironments on the continental shelf of the East China Sea. *Journal of Asian Earth Sciences* 18 (4), 441–452.
- Liu, J.P., Milliman, J.D., Gao, S., 2002. The Shandong mud wedge and post-glacial sediment accumulation in the Yellow Sea. *Geo-Marine Letters* 21 (4), 212–218.
- Liu, J.P., Milliman, J.D., Gao, S., Cheng, P., 2004. Holocene development of the Yellow River's subaqueous delta, North Yellow Sea. *Marine Geology* 209 (1–4), 45–67.
- Liu, J.P., Li, A.C., Xu, K.H., Yang, Z.S., Velozzi, D.M., Milliman, J.D., DeMaster, D.J., 2006. Sedimentary features of the Yangtze River-derived alongshore clinoform deposit in the East China Sea. *Continental Shelf Research* 26, 2141–2156.
- Liu, J.P., Xu, K.H., Li, A.C., Milliman, J.D., Velozzi, D.M., Xiao, S.B., Yang, Z.S., 2007a. Flux and fate of Yangtze River sediment delivered to the East China Sea. *Geomorphology* 85 (3–4), 208–224.
- Liu, Z.X., Berne, S., Saito, Y., Yu, H., Trentesaux, A., Uehara, K., Yin, P., Liu, J.P., Li, C., Hu, G., Wang, X., 2007b. Internal architecture and mobility of tidal sand ridges in the East China Sea. *Continental Shelf Research* 27 (13), 1820–1834.
- Liu, J.P., Liu, C.S., Xu, K.H., Milliman, J.D., Chiu, J.K., Kao, S.J., Lin, S.W., 2008a. Flux and fate of small mountainous rivers derived sediments into the Taiwan Strait. *Marine Geology* 256 (1–4), 65–76.
- Liu, Z., Tu, S., Colin, C., Liu, J.T., Huang, C.-Y., Selvaraj, K., Chen, C.A., Zhao, Y., Siringan, F.P., Boulay, S., Chen, Z., 2008b. Detrital fine-grained sediment contribution from Taiwan to the northern South China Sea and its relation to regional ocean circulation. *Marine Geology* 255 (3–4), 149–155.
- Liu, H., He, Q., Wang, Z., Weltje, G.J., Zhang, J., 2010b. Dynamics and spatial variability of near-bottom sediment exchange in the Yangtze Estuary, China. *Estuarine, Coastal and Shelf Science* 86, 322–330.
- Liu, J., Saito, Y., Kong, X.H., Wang, H., Xiang, L.H., Wen, C., Nakashima, R., 2010a. Sedimentary record of environmental evolution off the Yangtze River estuary, East China Sea, during the last 13,000 years, with special reference to the influence of the Yellow River on the Yangtze River delta during the last 600 years. *Quaternary Science Reviews* 29, 2424–2438.
- McCave, I.N., Tucholke, B.E., 1986. Deep current-controlled sedimentation in the western North Atlantic. In: Vogt, P.R., Tucholke, B.E. (Eds.), *The geology of North America*, Vol. M, The Western North Atlantic region. *Geol. Soc. America*, pp. 451–468.
- Meade, R.H., 1996. River-sediment inputs to major deltas. In: Milliman, J., Haq, B. (Eds.), *Sea-level rise and coastal subsidence*. Kluwer, London, pp. 63–85.
- Milliman, J.D., Meade, R.H., 1983. World-wide delivery of sediment to the oceans. *Journal of Geology* 91 (1), 1–21.
- Milliman, J.D., Syvitski, J.P.M., 1992. Geomorphic/tectonic control of sediment discharge to the ocean: The importance of small mountainous rivers. *Journal of Geology* 100 (5), 525–544.
- Milliman, J.D., Shen, H.-T., Yang, Z.-S., Meade, R.H., 1985. Transport and deposition of river sediment in the Changjiang estuary and adjacent continental shelf. *Continental Shelf Research* 4 (1–2), 37–45.
- Milliman, J.D., Lin, S.W., Kao, S.J., Liu, J.P., Liu, C.S., Chiu, J.K., Lin, Y.C., 2007. Short-term changes in seafloor character due to flood-derived hyperpycnal discharge: Typhoon Mindulle, Taiwan, July 2004. *Geology* 35 (9), 779–782.
- Mitchum Jr., R.M., Vail, P.R., Thompson, S., 1977. Seismic stratigraphy and global changes of sea level, Part 2: The depositional sequence as a basic unit for stratigraphic analysis. In: Payton, C.E. (Ed.), *Seismic stratigraphy – Application to hydrocarbon exploration*: American Association of Petroleum Geologists Memoir, 26, pp. 53–62.
- Oguri, K., Matsumoto, E., Yamada, M., Saito, Y., Iseki, K., 2003. Sediment accumulation rates and budgets of depositing particles of the East China Sea. *Deep Sea Research Part II: Topical Studies in Oceanography, Biogeochemical Cycle in the East China Sea* 50 (2), 513–528.
- Qin, Y.S., Zhao, Y.Y., Chen, L.R., Zhao, S.L., 1987. *Geology of the East China Sea*. China Science Press, Beijing. 290 pp.
- Sadler, P.M., 1981. Sediment accumulation rates and the completeness of stratigraphic sections. *Journal of Geology* 89, 569–584.
- Schaefer, D.W., Kunze, C.W., 1971. A clay mineral investigation of six cores from the Gulf of Mexico. *Marine Geology* 10, 69–85.
- Stuiver, M., Burr, G.S., Hughen, K.A., Kromer, B., McCormac, G., Van Der Plicht, J., Spurk, M., Reimer, P.J., Bard, E., Beck, J.W., 1998. INTCAL98 radiocarbon age calibration, 24,000–0 cal BP. *Radiocarbon* 40 (3), 1041–1083.
- Su, C.-C., Huh, C.-A., 2002. ^{210}Pb , ^{137}Cs and $^{239,240}\text{Pu}$ in East China Sea sediments: SOURCES, pathways and budgets of sediments and radionuclides. *Marine Geology* 183 (1–4), 163–178.
- Thompson, L.G., Mosley-Thompson, E., Davis, M.E., Bolzan, J.F., Dai, J., Yao, T., Gundestrup, N., Wu, X., Klien, L., Xie, Z., 1989. Holocene-Late pleistocene climatic ice core records for Qinghai-Tibetan plateau. *Science* 246, 474–477.
- Tucholke, B.E., 2002. The Greater Antilles Outer Ridge: Development of a distal sedimentary drift by deposition of fine-grained contourites. In: Stow, D.A.V., Pudsey, C.J., Howe, J.A., Faugeres, J.-C., Viana, A.R. (Eds.), *Deep-water contourite systems: Modern drifts and ancient series, seismic and sedimentary characteristics*: Geological Society London, Memoirs, 22, pp. 39–55.
- Tucholke, B.E., Hollister, C.D., Biscaye, P.E., Gardner, W.D., 1985. Abyssal current character determined from sediment bedforms on the Nova Scotian continental rise. *Marine Geology* 66, 43–57.
- Uehara, K., Saito, Y., 2003. Late Quaternary evolution of the Yellow/East China Sea tidal regime and its impacts on sediments dispersal and seafloor morphology. *Sedimentary Geology* 162 (1–2), 25–38.
- Uehara, K., Saito, Y., Hori, K., 2002. Paleotidal regime in the Changjiang (Yangtze) Estuary, the East China Sea, and the Yellow Sea at 6 ka and 10 ka estimated from a numerical model. *Marine Geology* 183 (1–4), 179–192.
- Wang, P., Sun, X., 1994. Last glacial maximum in China: Comparison between land and sea. *Catena* 23 (3–4), 341–353.
- Wang, Z., Saito, Y., Hori, K., Kitamura, A., Chen, Z., 2005. Yangtze offshore, China: Highly laminated sediments from the transition zone between subaqueous delta and the continental shelf. *Estuarine, Coastal and Shelf Science* 62 (1–2), 161–168.
- Wang, Z.H., Xu, H., Zhan, Q., Saito, Y., He, Z.F., Xie, J.L., Li, X., Dong, Y.H., 2010a. Lithological and palynological evidence of late Quaternary depositional environments in the subaqueous Yangtze delta, China. *Quaternary Research* 73, 550–562.
- Wang, Z.H., Li, M.T., Zhang, R.H., Zhuang, C.C., Liu, Y., Saito, Y., Xie, J.L., Li, B., 2010b. Impacts of human activity on the late Holocene development of the subaqueous Yangtze delta, China, as shown by magnetic properties and sediment accumulation rates. *The Holocene* 21 (3), 393–407. doi:10.1177/0959683610378885.
- Xia, X., Xie, Q., Li, Y., Li, B., Feng, Y., 1999. ^{137}Cs and ^{210}Pb profiles of the seabed cores along the East China Sea coast and their implications to sedimentary environment. *Donghai Marine Science* 17 (1), 20–27.
- Xia, X., Yang, H., Li, Y., Li, B., Pan, S., 2004. Modern sedimentation rates in the contiguous sea area of Changjiang Estuary and Hangzhou Bay. *Acta Sedimentologica Sinica* 22 (1), 130–135.
- Xiao, S., Li, A., Jiang, F., Li, T., Wan, S., Huang, P., 2004. Sedimentary record and climatic signal in the mud wedge of the inner shelf of East China Sea since 2 ka BP. *China Science Bulletin* 49 (21), 2233–2238.
- Xiao, S., Li, A., Chen, M., Liu, J., Jiang, F., Li, T., Xie, Q., Xiang, R., Chen, Z., 2005. Recent 8 ka mud records of the east Asian winter monsoon from the inner shelf of the East China Sea. *Journal of China University of Geosciences (Earth Science)* 30 (5), 573–581.
- Xu, K.H., 2006. Linking land to ocean: flux and fate of water and sediment from the Yangtze River to the East China Sea. Ph.D. dissertation Thesis, The College of William & Mary, 174 pp.
- Xu, K.H., Milliman, J.D., 2009. Seasonal variations of sediment discharge from the Yangtze River before and after impoundment of the Three Gorges Dam. *Geomorphology* 104 (3–4), 276–283.
- Xu, K.H., Milliman, J.D., Yang, Z.S., Wang, H.J., 2006. Yangtze sediment decline partly from Three Gorges Dam. *EOS Transactions* 87 (19), 185–190.
- Xu, K.H., Milliman, J.D., Yang, Z.S., Xu, H., 2007. Climatic and anthropogenic impacts on the water and sediment discharge from the Yangtze River (Changjiang), 1950–2005. In: Gupta, A. (Ed.), *Large rivers: Geomorphology and management*. John Wiley & Sons, pp. 609–626.
- Xu, F.J., Li, A.C., Xiao, S.B., Wan, S.M., Liu, J.G., Zhang, Y.C., 2009b. Paleoenvironmental evolution in the inner shelf of the East China Sea since the last deglaciation. *Acta Sedimentologica Sinica* 27 (1), 118–127 (in Chinese with English abstract).
- Xu, K.H., Milliman, J.D., Li, A.C., Liu, J.P., Kao, S.J., Wan, S.M., 2009a. Yangtze- and Taiwan-derived sediments in the inner shelf of East China Sea. *Continental Shelf Research* 29, 2240–2256. doi:10.1016/j.csr.2009.08.017.
- Xu, K.H., Milliman, J.D., Xu, H., 2010. Temporal trend of precipitation and runoff in major Chinese rivers since 1951. *Global and Planetary Change* 73, 219–232. doi:10.1016/j.gloplacha.2010.07.002.
- Ye, Y., Li, J., Song, L., 1981. Holocene stratigraphy and paleogeography in the near shore area of Wenzhou, Zhejiang Province. *Marine Practice* 4 (4), 32–37.
- Yi, S., Saito, Y., Zhao, Q., Wang, P., 2003. Vegetation and climate changes in the Changjiang (Yangtze River) Delta, China, during the past 13,000 years inferred from pollen records. *Quaternary Science Reviews* 22 (14), 1501–1519.
- Yi, S., Saito, Y., Chen, Z., Yang, D.Y., 2006. Palynological study on vegetation and climatic change in the subaqueous Changjiang (Yangtze River) delta, China, during the past about 1600 years. *Geosciences Journal* 10, 17–22.
- You, Z., Tang, J., Liao, L., 1993. Studies on clay mineral in sediment cores from western Taiwan Strait. *Journal of Oceanography in Taiwan Strait* 12 (1), 1–7 (in Chinese with English abstract).
- Yu, P., Li, N., 1992. The crust thermal flux of the East China Sea. *China Ocean Press*, Beijing. 127 pp.
- Zheng, Y., Kissel, C., Zheng, H.B., Laj, C., Wang, K., 2010. Sedimentation on the inner shelf of the East China Sea: Magnetic properties, diagenesis and paleoclimate implications. *Marine Geology* 268 (1–4), 34–42.